A non-bactericidal antimicrobial peptide provides protective effect against bacterial sepsis via regulation of antimicrobial immunity and vascular endothelial functions

Yanmei He[1†], Ting Lin[1†], Lixian Mu[1†], Xiaoyan Zhou[1], Yan Shen[1], Jiayi Yang[1], Haiyan Luo[1], Pengyao Liu[1], Lin Wei[2*], Jing Wu[1*], and Hailong Yang[1*]

[1] School of Basic Medical Sciences, Kunming Medical University, Kunming 650500, Yunnan, China

[2] School of Life Sciences, Anhui Medical University, Hefei 230032, Anhui, China

†These authors made equal contributions to this work.

*Authors to whom correspondence should be addressed:

1168 West Chunrong Road, Yuhua Avenue, Chenggong District, Kunming 650500, Yunnan, China

Tel: +86 871 65922852

Fax: +86 871 65922852

E-mail: weilin1005@126.com (LW) or wujing_205@163.com (JW) or jxauyhl@163.com (HY)

ABSTRACT

The anti-infective properties of bactericidal antimicrobial peptides (AMPs) have been extensively studied, but less information is available regarding the role and mechanisms of action of non-bactericidal AMPs in sepsis. Herein, a novel β-sheet cathelicidin antimicrobial peptide (Og-CATH) was identified from the frog *Odorrana grahami*. Intriguingly, Og-CATH showed no direct antimicrobial activity *in vitro,* but displayed prophylactic and therapeutic efficacy in *Staphylococcus aureus*, *Enterobacteriaceae coli*, or cecal ligation and puncture-induced septic mice. Neutrophils and monocytes/macrophages, but not T/B lymphocytes, were required for the protective efficacy of Og-CATH in mice. Og-CATH did not exhibit a direct chemoattractant effect on phagocytes, but it promoted macrophages and neutrophils trafficking to the infection site via chemokines secreted by P2X7 receptor-activated macrophages, and augmented their oxygen-independent bacterial killing functions via the enhancement of phagocytosis and neutrophils degranulation. Of note, Og-CATH also inhibited the production of tissue factor, a potent initiator of the extrinsic coagulation cascade, and up-regulated the expression of activated protein C, a physiological anticoagulant both in endothelial cells and in mice, which contribute to the reduction of pulmonary fibrin deposition and thrombosis in mice. Further investigation revealed that Og-CATH targeted the myeloid differentiation protein 2 (MD2), and inhibited the LPS-induced MyD88 recruitment to TLR4 in endothelial cells, thus attenuating endothelial barrier dysfunction during sepsis. Our data indicated that Og-CATH provides protective effects against sepsis through regulation of phagocytes

and endothelial functions. These findings enrich our understanding of the anti-infection mechanism of non-bactericidal AMPs, and show that Og-CATH is an excellent candidate for further therapeutic development of sepsis.

Keywords： antimicrobial peptide; antimicrobial immunity; endothelial functions; P2X7 receptor; myeloid differentiation protein 2 (MD2);

INTRODUCTION

Sepsis, a life-threatening condition that occurs due to dysregulated host responses to infection, globally accounts for an alarming annual toll of 48.9 million cases and 11 million deaths (Nedeva, 2021). Early appropriate antibiotic therapy is essential in sepsis, but the emergence of multidrug-resistant bacteria leads to the therapy failing to reduce mortality from severe infections (Team, 2013; Strich *et al.*, 2020). Antimicrobial peptides (AMPs) are gene-encoded and derive from precursor peptides through one or more proteolytic acti-vation steps. In recent years, they have attracted a considerable attention because of potential application to combat antimicrobial resistance, and AMPs with direct antimicrobial activity were considered as a potential solution for the treatment of bacterial sepsis (Mookherjee *et al.*, 2007). However, increasing evidence indicates that the anti-infective efficacy of AMPs *in vivo* may largely be attributed to their immunomodulatory activity rather than direct antimicrobial activity which is often severely impaired in the presence of monovalent and divalent salts, and various host factors such as negatively charged polysaccharides, glycosaminoglycans, F-actin and apolipoproteins (Segal, 2005; Mookherjee and

Hancock, 2007; Teng *et al.*, 2017; Alford *et al.*, 2020; Herb and Schramm, 2021). This has increased interest in the development of new anti-infective strategies such as selective modulation of host innate immune functions. The cathelicidin family AMPs are a class of essential gene-encoded peptides that are identified exclusively in many sepcies. These peptides are effector molecules of host innate immunity that can provide a first line of defense against pathogens, and offer a promising approach to treat infections. Although anti-infective potential of bactericidal cathelicidins have been well characterized, the structure-activity relationships of the non-bactericidal cathelicidins are poorly understood.

Sepsis is the culmination of complex crosstalk between the invading pathogens and the host immune, inflammatory, and blood clotting. A number of studies have been focused on the modulation of the host innate immune and inflammatory response for AMPs in sepsis (Li *et al.*, 2013; Cai *et al.*, 2018; Nagaoka *et al.*, 2020; Wu *et al.*, 2021). However, there is limited understanding of regulation of hemostatic system for these molecules. Endothelial cells (ECs), at the interface between inflammation and coagulation in sepsis, are vital for vascular homeostasis, inflammatory modulation, and maintaining barrier integrity. Endotoxins or the pathogenesis of sepsis can not only cause the disturbance of the endothelial barrier, but also stimulate endothelial cells to express tissue factor that initiates the coagulation cascade. Fibrinogen is then transformed into fibrin, resulting to microvascular thrombosis and further amplifying tissue injury (Aird, 2001; van der Poll and Parker, 2020; Iba *et al.*, 2023). Studies underscore that it is essential to recognize the substantial changes in the endothelium

during sepsis, as it remains a crucial target for the treatment of sepsis. However, whether these AMPs, especially non-bactericidal AMPs can modulate the endothelial cell functions during sepsis, is still not fully understood.

Herein, we identified a cathelicidin AMP (Og-CATH) from the amphibian *O. grahami*. Stability experiments of Og-CATH, including thermal stability, serum stability and salt stability, were tested by high-performance liquid chromatography (HPLC). Circular dichroism (CD) spectroscopy was performed to analyze the secondary structure of Og-CATH. Subsequently, the antimicrobial ability, and prophylactic and therapeutic efficacy of Og-CATH were examined both *in vivo* and *in vitro*. The underlying molecular mechanisms of Og-CATH including its effects on the phagocyte-mediated bacterial killing functions were investigated. Furthermore, we explored the activities of Og-CATH on coagulation cascade, platelet functionality, thrombosis, as well as procoagulant and anticoagulant status of endothelial cells. We also evaluated the regulatory effects of Og-CATH on endothelial inflammation, apoptosis, and barrier function and explored the detailed mechanisms, including its target and downstream pathways.

MATERIALS AND METHODS

Ethics statement

All animal experiments were approved by the Institutional Animal Care and Use Ethics Committee of Kunming Medical University (IACUC approval number: KMMU 20221220). All studies using animals were designed in keeping with the 3Rs (replacement, reduction and refinement) principles.

Frog collection

Adult specimens of *O. grahami* (21-30 g) were captured in Lijiang County, Yunnan Province, in southwest China. After being collected, frogs were placed in a plastic container until use.

cDNA Cloning and Peptide Synthesis

The extraction of total RNA and construction of cDNA library from *O. grahami* skin were carried out following the previously procedure (Yang *et al.*, 2017). An antisense degenerate primer (5'- TTGT CTGC CTCC TCGG CTTCC3') was designed based on the conserved cathelin domain sequence in amphibians, and conjuncted with the 5'-PCR primer provided by the cDNA library construction kit. To analyze the full cDNA sequence that encodes the Og-CATH precursor, a sense primer (5'- ATGG CGCT CGCT GCTG CACTC-3') was designed and combined with 3' PCR primer (5'-ATTC TAGA GGCC GAGG CGGCCG-3') including in the kit. The PCR conditions included an initial step at 95°C for 2 min, followed by 30 cycles of denaturation at 92°C for 10 s, annealing at 50°C for 30 s, extension at 72°C for 40 s, and a final extension at 72°C for 10 min.

Og-CATH (AGRRRNRPPGRPRFPGLNNPIAGIPGRK) and the scrambled version of Og-CATH called sOg-CATH (FPRNRAKPGRIRPGRPNGARLNPIRGGP) were synthesized by by Synpeptide Bio-Tech Co. (Nanjing, China), and the purity was >95% analyzed by HPLC.

Cells, bacteria, and mice

MPMs (Mouse primary peritoneal macrophages) and BMDNs (bone marrow-derived

neutrophils) were obtained from male C57BL/6 mice using the method described in previous study (Kawasaki and Kawai, 2014). The cells were grown in RPMI 1640 medium (2% fetal bovine serum (FBS), 1% penicillin-streptomycin). Human umbilical vein endothelial cells (HUVECs) and human monocytic leukemia cell line 1 (THP-1) cells were obtained from the Institute of Zoology, Chinese Academy of Sciences (Kunming, China), and cultured in DMEM medium (10% FBS and 1% penicillin-streptomycin).

Microbial including Gram-positive and Gram-negative bacteria, as well as fungi were growth at a temperature of 37℃ in Luria-Bertani (LB) liquid medium.

Male C57BL/6 mice (18-22 g) and male BALB/c mice (18-22 g) were acquired from the Laboratory Animal Department of Kunming Medical University (Kunming, China). All procedures were performed with in the Yunnan Institutes of Health guidelines.

Bacterial infection models

O. grahami (21-30 g, $n = 4$) and C57BL/6 male mice (18-22 g, $n = 4$) were administered with 10 mg/kg Og-CATH via intraperitoneal injection 4 h before or after *S. aureus* and *E. coli* inoculation (10^8 CFU/frog, 2×10^8 CFU/mouse)). Peritoneal lavage fluid was obtained for bacterial counts at 24 h after the bacterial inoculation.

For CLP-induced septic mice, C57BL/6 male mice (18-22 g) received an intraperitoneal or intravenous injection of 10 mg/kg Og-CATH, sOg-CATH or Meropenem (10 mg/kg) 4 h before or after CLP. The CLP operation was performed according to previous method (Rittirsch *et al.*, 2009). The survival rate of infected mice for 7 days was recorded, and then peripheral blood and organs (lungs, livers, and

kidneys) were obtained after 24 h with CLP operations for bacterial loads and pro-inflammatory mediators (TNF-α, IL-1β, IL-6) (Multi Sciences, Hangzhou, China) assay. Meanwhile, the lungs, livers, and kidneys tissues were fixed with a 4% solution of paraformaldehyde for 24 h. Subsequently, the tissues were cut into sections and subjected to staining using an H&E kit (Solarbio, China). Addtionally, alanine aminotransferase (ALT) and creatinine levels in serum were also quantified with assay kits. Notably, n = 6 mice were used per group for survival studies. For other endpoint analyses (bacterial burden, cytokines, histology), data was obtained from n = 4 mice per group.

Chemotaxis assay *in vivo*

O. grahami (21-30 g, n = 4) were administered Og-CATH (10 mg/kg) or PBS via intraperitoneal injection. At 0, 6, 12, 24, and 48 h after injection, the peritoneal lavage cells were gathered and enumerated with hemocytometer. Then, the cells were observed using microscope following performed Wright-Giemsa staining.

Male C57BL/6 mice (18-22 g, n = 4) received an intraperitoneal injection of Og-CATH (10 mg/kg), sOg-CATH (10 mg/kg) or meropenem (10 mg/kg). Peritoneal lavage cells were obtained at 12, 24, and 48 h after peptide or meropenem administration to determine cell types. PBS with equal volume served as control. FTIC anti-mouse Gr-1 antibody and PE anti-mouse F4/80 antibody were used to analyze myeloid cells. These cells were stained with corresponding antibody at room temperature for 30 min, then washed with PBS. Subsequently, they were analyzed using a flow cytometer FACS Canto II and FlowJo seven software.

Chemotaxis assay *in vitro*

For direct chemotaxis studies, neutrophils or macrophages (7×10^6 cells/mL) was placed in the top chamber of a transwell in a 24-well plate. The lower chamber was filled with 500 μL of 2% FBS RPMI 1640 containing Og-CATH at concentrations of 25, 50, and 100 μg/mL (dissolved in PBS) or PBS as a vehicle control. After 8 h of incubation, the cells that had moved to the bottom chamber were collected and quantified using a hemocytometer. The number of cells in the lower chamber corresponded to the amount of migration (Xue *et al.*, 2023).

Indirect chemotaxis were studied using a co-culture system based on the method described earlier (Liu *et al.*, 2023). In brief, macrophages (4×10^6 cells/mL) were inoculated into the lower chamber 2 h prior to co-incubation. Og-CATH (25, 50, and 100 μg/mL, dissolved in PBS) and PBS (vehicle) were placed to the lower chamber. Next, neutrophils or macrophages suspension (100 μL/well) with a final density of 7×10^6 cells/mL was seeded to the upper chamber of transwell filters. Following incubation for 8 h in an incubator, the number of cells in the upper chamber was counted using a hemocytometer. Migration was assessed by measuring the reduction in cell count in the upper chamber.

Myeloid cell-deficient septic mice model

For macrophage/monocyte-deficient model, C57BL/6 male mice (18-22 g, $n = 4$) were intraperitoneally administered 200 μL of clodronate liposomes (FormuMax Scientific, CA) 48 h before CLP (Cai *et al.*, 2018). For the neutropenia model, mice were given 200 mg/kg and 150 mg/kg doses of cyclophosphamide (Sigma, USA) via

intraperitoneal injection on days 0 and 3, respectively (Lei *et al.*, 2020). All deficient mice were injected with Og-CATH (10 mg/kg) intraperitoneally, and peritoneal cells were harvested at the times specified (0, 6, 12, 24, and 48 h) after administration to analyze the cell types using flow cytometry. Meanwhile, CLP was performed to induce sepsis in deficient mice, and Og-CATH was intraperitoneally injected into mice at 4 h before or after CLP operation. The bacterial burden was detected in the peritoneal lavage at 24 h after CLP.

Regulatory effects of Og-CATH on macrophages

MPMs were cultured in 6-well plates and exposed to Og-CATH (100 μg/mL), sOg-CATH (100 μg/mL) or meropenem (1 mg/mL). After cultured for 6 h at a cell culture incubator, total RNA in the cells was extracted using Trizol reagent. cDNA was synthesized with cDNA Synthesis Kit (Thermo Fisher Scientific Inc.), quantitative real-time PCR (qRT-PCR) was performed to analyze CXCL-and CCL- chemkines using the Bio-Rad CFX96 real-time system as described previously(Li *et al.*, 2021). In mice, C57BL/6 mice (male, 18-22 g, n = 4) were given Og-CATH (10 mg/kg) via intraperitoneal injection, and peritoneal lavage was harvested at 0, 6, 12, 24, and 48 h after injection. The levels of chemokines in the cultured cell supernatant and the mouse peritoneal lavage were analyzed with ELISA kits (Multi Sciences, China). The primers listed in Supplementary Table S2.

For pharmacological inhibitors experiments, Pertussis toxin (Gi-protein inhibitor) (from Invitrogen, USA), KN62 (P2X7 receptor) (from Invitrogen, USA), MTS510 (TLR 4 inhibitor) (from Sigma-Aldrich) and WRW4 (FLPR-1 antagonist) (GL

Biochem, China) were used to explore receptor of chemokines expression induced by Og-CATH. All inhibitors were dissolved in DMSO. For receptor studies, the MPMs were added and adhered to 24-well plates at a density of 2×10^5 cells/well. Then, cells were pretreated with KN-62 (2 μM), WRW4 (10 μg/mL) and MTS510 (10 μg/mL) for 1 h, respectively. Then the cells were stimulated with Og-CATH (100 μg/mL) for 6 h, and the level of CXCL1, CXCL2, CXCL3 and CCL2 in cell culture supernatant was analyzed using ELISA kits (Multi Sciences, China)

Regulatory effects of Og-CATH on neutrophils

For phagocytosis detect, BMDNs were pre-treatment with Og-CATH (25, 50, and 100 μg/mL), sOg-CATH (100 μg/mL) or PBS for 2 h. Meanwhile, *S. aureus* and *E. coli* were pre-labeled using CFSE fluorescent dye at a concentration of 10 μM in PBS, which lasted at a temperature of 37°C for 30 min. Sequentially, to immobilize the bacteria, 1% paraformaldehyde (Solarbio, China) was mixed with PBS containing bacteria and incubated for 1 h. Bacteria were washed twice with PBS. Bacterial particles marked with CFSE were used to treat the cells. After incubation for 1 h, the cells were washed, the extracellular fluorescence were quenched with 15 mg/mL of trypan blue (Solarbio, China). Subsequently, the CFSE fluorescence was examined using flow cytometry to assess the bacterial particles' phagocytic uptake.

To assess the bactericidal activity of neutrophils, BMNDs (1×10^6 cells/well) were seeded to 24-well plates. For ROS detection, cells were treated with Og-CATH (100 μg/mL), sOg-CATH (100 μg/mL) or PBS for 20 min at 37℃. And cells were collected and stained with 5 μM DCFH-DA in PBS at 37°C for 30 min. Flow cytometry was used

to measure the fluorescence, and the ROS levels were calculated as a multiple of the average fluorescence intensity (MFI) resulting from PBS treatment. For NO assay, cells were treated with Og-CATH (25, 50, and 100 μg/mL), sOg-CATH (100 μg/mL) or 100 ng/mL LPS for 6 h at a cell culture incubator. Nitrite levels in the supernatants were measured using Griess reagent as the manufacturer's instructions (Beyotime, China). For degranulation assay, BMDNs were treated with different doses of Og-CATH (25, 50, and 100 μg/mL), sOg-CATH (100 μg/mL) or PBS for 6 h at a cell culture incubator. BPI, Lactoferrin and MMP-9 levels in cells supernatants were assessed using ELISA kits (Fine Biotech, Wuhan, China). For NETs production assays, BMDNs were exposed to Og-CATH (100 μg/mL), PMA (15 μg/mL), sOg-CATH (100 μg/mL) or PBS, followed by staining with DAPI or anti-Cit-H3 (1:100). The nuclei and NETs were visualized under a confocal microscope.

Regulatory effects of Og-CATH on HUVECs

To assess cytokines generation, HUVECs were seeded in a 24-well plate and cultured until they reached 80% confluence. Cells were then incubated at 37°C for 24 h with or without 10 μg/mL LPS and in the presence of Og-CATH (25, 50, and 100 μg/mL). The concentrations of TNF-α, IL-6, and IL-1β in the supernatants were measured using ELISA kits (Multi Sciences, Hangzhou, China).

For apoptosis assays, HUVECs were plated in a 6-well plate and incubated at 37°C for 24 h with Og-CATH (25, 50, and 100 μg/mL) and LPS (10 μg/mL). After two washes with PBS, the cells were collected using trypsinization. Cell staining was conducted with an apoptosis detection kit (Biyuntian, China), and the apoptosis rates

were assessed with a FACS Canto II flow cytometer and analyzed using Flowjo software. Additionally, the total protein was extracted for endothelial barrier integrity assay by western blot analysis. The following primary antibodies were used: β-actin (Rabbit Monoclonal, Clone 13E5, CST, Cat. #4970, USA; 1:4000), E-cadherin (Mouse Monoclonal, Clone 6B10-F4-G10, ZENBIO, Cat. #201283, China; 1:1000), occludin (Rabbit Monoclonal, Clone R08-6C4, ZENBIO, Cat. #R381549, China; 1:1000), and ZO-1 (Rabbit Polyclonal, ZENBIO, Cat. #511417, China; 1:1000), IKBα (Mouse Monoclonal, Clone L35A5, CST, Cat. #4814T, USA; 1:2000), Phospho-IkappaB alpha (Ser32) (Rabbit Monoclonal, Clone 14D4, CST, Cat. #2859T, USA; 1:2000), IKKβ (Mouse Monoclonal, Clone D30C6, CST, Cat. #8943T, USA; 1:2000), Phospho-IKK alpha/beta (Ser176/180) (Rabbit Monoclonal, Clone 16A6, CST, Cat. #2697T, USA; 1:2000), Phospho-NF-kappaB p65 (Ser536) (Rabbit Monoclonal, Clone 93H1, CST, Cat. #3033, USA; 1:2000), NF-kappaB p65 (Rabbit Monoclonal, Clone D14E12, CST, Cat. #8242, USA; 1:2000). Quantitative analysis was conducted with ImageJ software.

To investigate pro-coagulation/anti-coagulation activity, HUVECs were plated in a 6-well plate and grown until 80% confluence. The cells were then incubated at 37°C for 24 h with or without 10 μg/mL LPS and in the presence of Og-CATH (25, 50 and 100 μg/mL), sOg-CATH (100 μg/mL) or meropenem (1 mg/mL) . Meanwhile, male C57BL/6 mice (18-22 g, n = 4) were given PBS or 10 mg/kg Og-CATH via intraperitoneal injection 4 h before or after the CLP procedure. Lung tissue of mice were collected after 24 h with Og-CATH treatment. Western blot were used to measure TF (Tissue Factor) (Rabbit Monoclonal, Clone R07-9O1, ZENBIO, Cat. #381361,

China; 1:1000), TM (thrombomodulin) (Rabbit Monoclonal, Clone R02-1G1, ZENBIO, Cat. #R25903, China; 1:1000), EPCR (endothelial protein C receptor) (Rabbit Monoclonal, Clone EPR25647-49, Abcam, Cat. #AB300565, USA; 1:2000), and APC (active protein C) (Rabbit Monoclonal, Clone EP701Y, Abcam, Cat. #ab40778, USA; 1:2000) in HUVEC and lung tissue, following our previously described method (He *et al.*, 2024).

Co-immunoprecipitation (Co-IP) assay

HUVECs were seeded into 6-well culture plates and grown until approximately 80% confluence. Cells were then incubated at 37°C for 1 h in the presence or absence of LPS (10 μg/mL) and Og-CATH (100 μg/mL). After treatment, cells were washed twice with ice-cold PBS and lysed in 1 mL Co-IP lysis buffer supplemented with a complete protease inhibitor cocktail and 1 mM phenylmethylsulfonyl fluoride (PMSF). Lysis was performed on ice for 30 min. The lysates were then centrifuged at 12,000 × g for 12 min at 4°C to remove cellular debris. The supernatant was incubated with anti-TLR4 (Mouse Monoclonal, Clone 3G9A4, Proteintech, Cat. #66350-1-Ig, China; 1:200) antibody at 4°C overnight. A parallel immunoprecipitation was carried out using IgG, as a negative control. Subsequently, pre-washed magnetic beads were added and incubated at room temperature for 1 h. The beads were washed three times with Tris-buffered saline (TBS) and then boiled in SDS sample buffer at 95°C for 5 min. The samples were then subjected to Western blot analysis. Additional antibodies used for immunoblotting include β-actin (Rabbit Monoclonal, Clone 13E5, CST, Cat. #4970, USA; 1:4000), TLR4 (Mouse Monoclonal, Clone

3G9A4, Proteintech, Cat. #66350-1-Ig, China; 1:2000), MD2 (Rabbit Polyclonal, abcam, Cat. #ab24182, USA; 1:2000), and MyD88 (Mouse Monoclonal, Clone 2E10D3, Proteintech, Cat. #67969-1-Ig, China; 1:1000).

Affinity measurement

The interactions between Og-CATH and TLR4/MD2/LPS were investigated using FortéBio Octet system (FortéBio, Inc., Menlo Park, CA). Og-CATH was dialyzed in PBST (PBS + 0.01% Tween-20) and diluted to 25 μg/mL. AR2G biosensor tips (FortéBio, Inc., Menlo Park, CA) were pre-wetted in PBST for 10 min before use. The Og-CATH was fixed to the AR2G biosensor according to the manufacturer. The sensors loading with PBS were used as the control group. TLR4 (MCE, 1 and 10 μM) , MD2 (abcam, 0.046-0.733 mM) or LPS (Sigma, 1 and 10 μg/mL) were dispensed into 96-well microtiter plates (Millipore, Billerica, MA) at a volume of 150 μL per well. The detection conditions used were (1) baseline 120 s; (2) activation 120 s; (3) loading 90 s; (4) quench 120 s; (5) wash 120 s; (6) association 360 s; (7) dissociation 360 s. The equilibrium dissociation constant (KD) were measured by the Octet Analysis software.

Isothermal titration calorimetry (ITC) analysis

The binding affinity between Og-CATH and MD2 was measured using a PEAQ-ITC instrument (Malvern Pananalytical Inc., MA) via direct titration. Briefly, Og-CATH (dissolved in dd H_2O) was diluted to a final concentration of 20 μM, and MD2 protein was diluted to 2 μM. During the ITC experiment, the Og-CATH solution was loaded into the syringe, while the MD2 protein solution was placed in the sample cell of the calorimeter. Each titration consisted of 19 sequential injections of the ligand (Og-

CATH) into the MD2-containing cell. The duration of each injection was 150 s, with a constant stirring speed of 750 rpm. The measurements were carried out at 25°C.

Cellular thermal shift assay (CETSA)

HUVECs were cultured in 6-well plates, harvested and washed twice with cold PBS. The collected cells were resuspended in RIPA lysis buffer supplemented with a complete protease inhibitor cocktail. Cell lysates were centrifuged at 12,000 × g for 15 min at 4°C, and the supernatants were collected. The lysates were then incubated with either Og-CATH (100 μg/mL) or PBS at room temperature for 1 h. After incubation, the treated lysates were aliquoted into equal volumes (100 μL per tube) and subjected to heat treatment at different temperatures (50°C, 55°C, 60°C, 65°C, 70°C, 75°C, and 80°C) for 5 min. After heating, all samples were cooled at room temperature for 3 min. The samples were subsequently centrifuged at 20,000 × g for 20 min at 4°C to separate the soluble fractions from precipitates. Supernatants were collected for subsequent immunoblot analysis. The antibody involved is MD2 (Rabbit Polyclonal, abcam, Cat. #ab24182, USA; 1:2000).

Molecular docking

The interaction between Og-CATH and MD2 was investigated based on the crystal structure of the TLR4/MD2 complex (PDB ID: 3FXI). During protein preparation, all bound TLR4, LPS, ions, and water molecules were removed to isolate the MD2 component. The structure of Og-CATH was obtained and processed using LigPrep for energy minimization and ligand preparation. The molecular docking was performed using the HPEPDOCK server (publicly accessible at

http://huanglab.phys.hust.edu.cn/hpepdock/), with all simulations conducted under the server's default parameter settings. All subsequent molecular visualization, structural analysis, and figure generation were carried out using PyMOL version 2.5.0.

Antithrombotic activity assays in mice

For fibrin detection, male C57BL/6 mice (18-22 g, n = 4) were given PBS or 10 mg/kg Og-CATH, sOg-CATH or meropenem via intraperitoneal injection 4 h before or after the CLP procedure. Lung tissue of mice were collected after 24 h for fibrin detection by utilizing an immunohistochemistry assay kit (Boster Biological technology Ltd., China) according to the manufacturer's in structions. The primary antibody used were anti-Fibrinogen (Rabbit Monoclonal, Clone EPR2919, Abcam, Cat. # ab92572, USA; 1:2000). Meanwhile, q-PCR were also performed to detect the levels of TF, APC, uPA (urokinase plasminogen activator) and PAI-1 (inhibitor plasminogen activator inhibitor 1) gene in the mouse lung tissue. Primers sequences are shown in S2 Table.

For $FeCl_3$-induced carotid artery thrombosis model, male C57BL/6 mice (18-22 g, n = 4) were subjected to intraperitoneal injections of 0.9% saline, heparin (1000 U/kg), sOg-CATH (10 mg/kg) or meropenem (10 mg/kg) or Og-CATH (10 mg/kg). 1 h after treatment, the mice were fully anesthetized and secured in a supine position. After shaving the neck area, the left common carotid artery was carefully exposed and isolated over a length of approximately 1 cm. A PVDF membrane-backed waterproof blue paper was placed underneath the artery to minimize background interference. A filter paper saturated with 10% (w/v) $FeCl_3$ solution was then applied to the artery for

30-60 s. Residual $FeCl_3$ was completely washed away with PBS. Blood flow was monitored for 30 min with a laser speckle imaging system, and the time to full occlusion of the vessel was measured. Data were analyzed using the system's dedicated software.

For carrageenan-induced tail thrombosis model, male BALB/c mice (18-22 g, n = 4) were administered intravenous injections of 0.9% saline, heparin (1000 U/kg), Og-CATH (10 mg/kg), sOg-CATH (10 mg/kg) or meropenem (10 mg/kg) via the tail vein. 1 h later, the mice was intraperitoneally injected with 0.25 mL of 1% carrageenan to induce tail thrombosis, with the temperature maintained at 17°C. Tail thrombus length was measured at 6, 12, 24, and 48 h post-induction.

Statistical analysis

The data were plotted using GraphPad Prism 8 software, with error bars indicating the standard error of the mean. One-way analysis of variance (ANOVA) followed by Dunnett's post hoc test was used to compare means. Additionally, to compare two groups, a statistical analysis was carried out using an unpaired two-tailed Student's t-test. The data are expressed as mean ± SD from three independent experiments or four mice. Statistical significance was noted in Figures or legends where appropriate. * $P < 0.05$ or $^{\#} P < 0.05$ was considered statistically significant.

RESULTS

A novel β-sheet cathelicidin was identified from the skin of frog O. grahami, and it has good stability under physiological condition

The cDNA sequence that encodes cathelicidin precursor was acquired by utilizing the

PCR-based cDNA cloning technique from the skin cDNA library of *O. grahami* (GenBank accession number OQ870535). The inferred precursor consists of 150 amino acid residues, which encompass a predicted 20-residue signal peptide, a conserved 102-residue cathelin domain, and a 28-residue mature peptide (designated as Og-CATH) at the C-terminal. Supplementary Figure S1A shows the complete amino acid sequence of Og-CATH. The mature peptide possessed 8 strongly basic residues (7 Arg and 1 Lys). Og-CATH has a mass of 3.08 kDa and a pI of 12.78. A BLAST analysis indicated that the Og-CATH precursor is part of the cathelicidin family, featuring a conserved cathelin domain and a variable C-terminal region (Supplementary Figure S1B). The secondary structure of Og-CATH was analyzed by Circular dichroism (CD) spectroscopy to test the conformational change of the peptide in aqueous (deionized water) and membrane-mimetic conditions (30-120 mM sodium dodecyl sulfate). As indicated in Supplementary Figure S1C, the results showed that the secondary structure of Og-CATH is mainly β-sheet (46.41-49.5%) both in sodium dodecyl sulfate (SDS) and H_2O solution. Subsequently, peptide stability is one of the most important parameters in the development of peptide therapeutics. Thus, we detected the stability of Og-CATH using HPLC, including thermal stability, serum stability and salt stability. As shown in Supplementary Figure S1D, 50-400mM NaCl treatment had no significant effect on the stability of Og-CATH. Similarly, Og-CATH maintained its structure after incubation at 37℃ for up to 7 days, repeated multigelation at -80℃ for 10 times or boiling at 100℃ for 1 h. Additionally, after incubating with fresh mouse serum, Og-CATH was gradually degraded over time, and

the remaining peptide was approximately 71.7% at 2 h and 42.6% at 4 h. These results indicated that Og-CATH has good stability under physiological condition.

Og-CATH lacks direct antimicrobial effects but it can prevent and treat bacterial infection in *O. graham* and mice

Cathelicidins were originally extensively studied due to their broad spectrum antimicrobial properties (Izadpanah and Gallo, 2005). Therefore, the *in vitro* antimicrobial ability of Og-CATH was initially assessed through MIC assay. The results showed that 200 μg/mL Og-CATH didn't exhibit direct antimicrobial effects against the detected standard or drug-resistant bacteria (a total of 17 strains), including Gram-negative bacteria, Gram-positive bacteria and fungi (Supplementary Table S1). In time-kill and metabolic activity investigations, 200 μg/mL Og-CATH does not decrease the CFUs and metabolic activity of *S. aureus*, *E. coli*, MRSA, and CREC following the cultivation for 1, 2, 3, and 4 h, respectively (Figure 1A, B). Similarly, the morphology of *S. aureus* and *E. coli* remained unchanged after incubation for 1 h with Og-CATH (200 μg/mL), as shown in Figure 1C. And the positive control peptide LL-37 (2×MIC), the only single human cathelicidin (Nagaoka *et al.*, 2020), markedly decreased bacterial CFUs and metabolic activity, as well as altered bacterial surface morphology (Figure 1A-C).

To investigate the antimicrobial activity of Og-CATH *in vivo*, *O. grahami* (21-30 g, n = 4) and C57BL/6 male mice (18-22 g, n = 4) were intraperitoneally injected with 10 mg/kg Og-CATH before (-4 h) or after (+4 h) inoculation with *S. aureus* or *E. coli* inoculation. The bacterial counts in frog or mouse peritoneal lavage were detected at

24 h after the bacterial challenge. Figure 1D showed that Og-CATH evidently decreased bacterial CFUs in frog and mouse infection models.

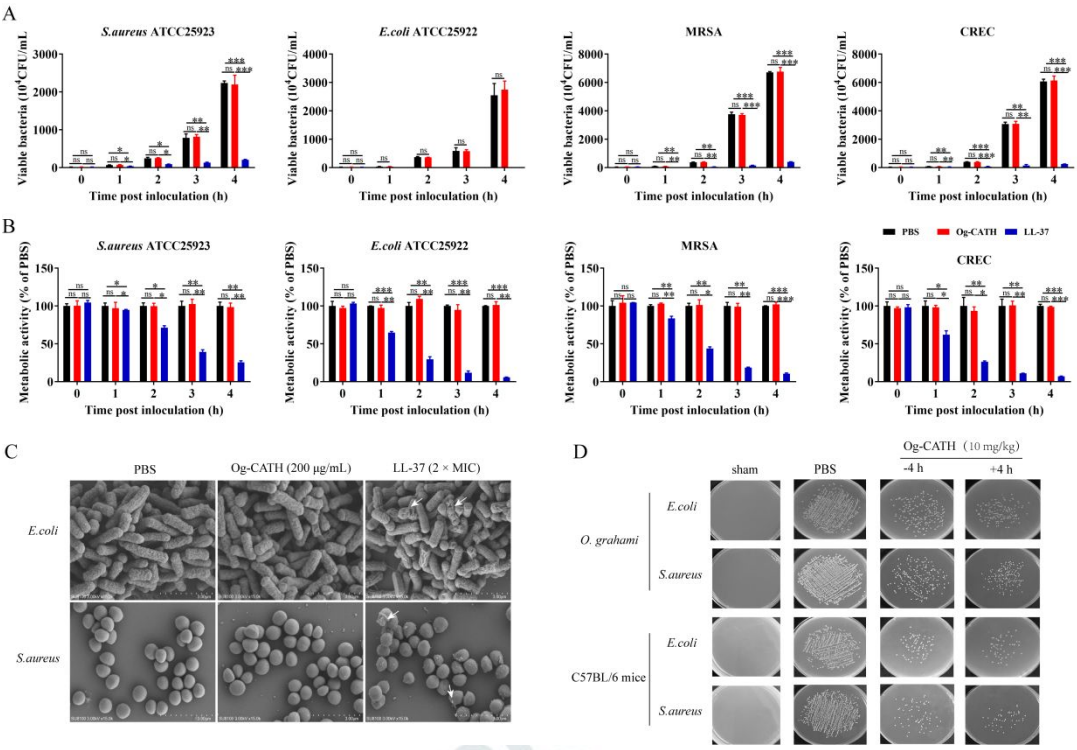

Figure 1 Og-CATH does not possess direct antimicrobial activity, but it can prevent and treat bacterial infections in *O. graham* and mice

A: Killing kinetic analysis of *S. aureus*, *E. coli*, MRSA and CREC. B: Metabolic activity of *S. aureus*, *E. coli*, MRSA and CREC. C: SEM analysis of *S. aureus* and *E. coli*. LL-37 (2×MIC) served as positive control. D: *in vivo* anti-microbial ability in *O. graham* and mice. *O. grahami* (n = 4) or mice (n = 4) were administered Og-CATH (10 mg/kg) via intraperitoneal injection 4 h before (-4 h) or 4 h after (+4 h) bacterial (*S. aureus* and *E. coli*) infection. Peritoneal lavage fluid was harvested for bacterial counts at 24 h after *S. aureus* and *E. coli* infection. * $P < 0.05$, ** $P < 0.01$, *** $P < 0.001$, ns, no significant difference. The mean ± SD of the values, obtained from three independent experiments, was presented.

Og-CATH protects mice against sepsis and sepsis-induced multiple organ failure

To further verify the possible mechanism of Og-CATH in combating bacterial infection, we initially assessed the toxicity and immunogenicity of Og-CATH both *in vitro* and *in vivo*. The results are shown in Supplementary Figure S2, Og-CATH within tested concentration did not show any toxic effects and immunogenicity on mammalian cells and mice up to 200 μg/mL concentration. As the most severe forms of bacterial infections, CLP causes poly-microbial infection within the peritoneal cavity that can result in organ failure and death (Dejager *et al.*, 2011). Thus, we subsequently investigated if Og-CATH exhibits protection against CLP-induced sepsis in mice (Figure 2A), similar to what was observed in mice infected by bacteria. Figure 2B shows that administering Og-CATH (10 mg/kg) or meropenem (positive control, 10 mg/kg) through intraperitoneal injection either prior to (-4 h) or after (+4 h) CLP operation greatly enhanced the mouse survival rates with CLP operation, compared with mice treated with sham. As shown in Figure 2C, Og-CATH and meropenem (10 mg/kg) treatment before or after CLP operation also significantly ameliorated the multiple organ damage caused by sepsis, and reduced the bacterial load and pro-inflammatory mediators (TNF-α, IL-6, and IL-1β) levels in kidney, liver, lung and serum of mice as compared to PBS treatment (Figure 2D, H; Supplementary Figure S3). In addition, the kidney, liver and lung tissues of septic mice exhibited markedly damage characterized by hemorrhage, extensive edema, and infiltration of inflammatory cells. Og-CATH or meropenem treatment significantly alleviated these injuries (Figure 2I). Furthermore, the ratio of wet to dry lung weights, and serum levels of liver and kidney function markers (ALT and creatinine)

in septic mice were significantly increased relative to sham operation (Figure 2J-L), and the treatment of Og-CATH and meropenem effectively decreased these elevated markers. However, in the above-described experiments, sOg-CATH, a scrambled version of Og-CATH, did not show a significant protective effect.

To evaluate the impact of different administration routes on the anti-sepsis effect of Og-CATH, we also investigated the preventive and therapeutic effects of intravenously administered Og-CATH. As illustrated in Supplementary Figure S4, administering Og-CATH (10 mg/kg) through intravenous injection either prior to (-4 h) or after (+4 h) CLP operation also enhanced the mouse survival rates with CLP operation. This finding is consistent with our observations from *in vitro* serum stability experiments, which demonstrated that Og-CATH retains at least 40% of its biological activity after four hours of co-incubation with mouse serum.

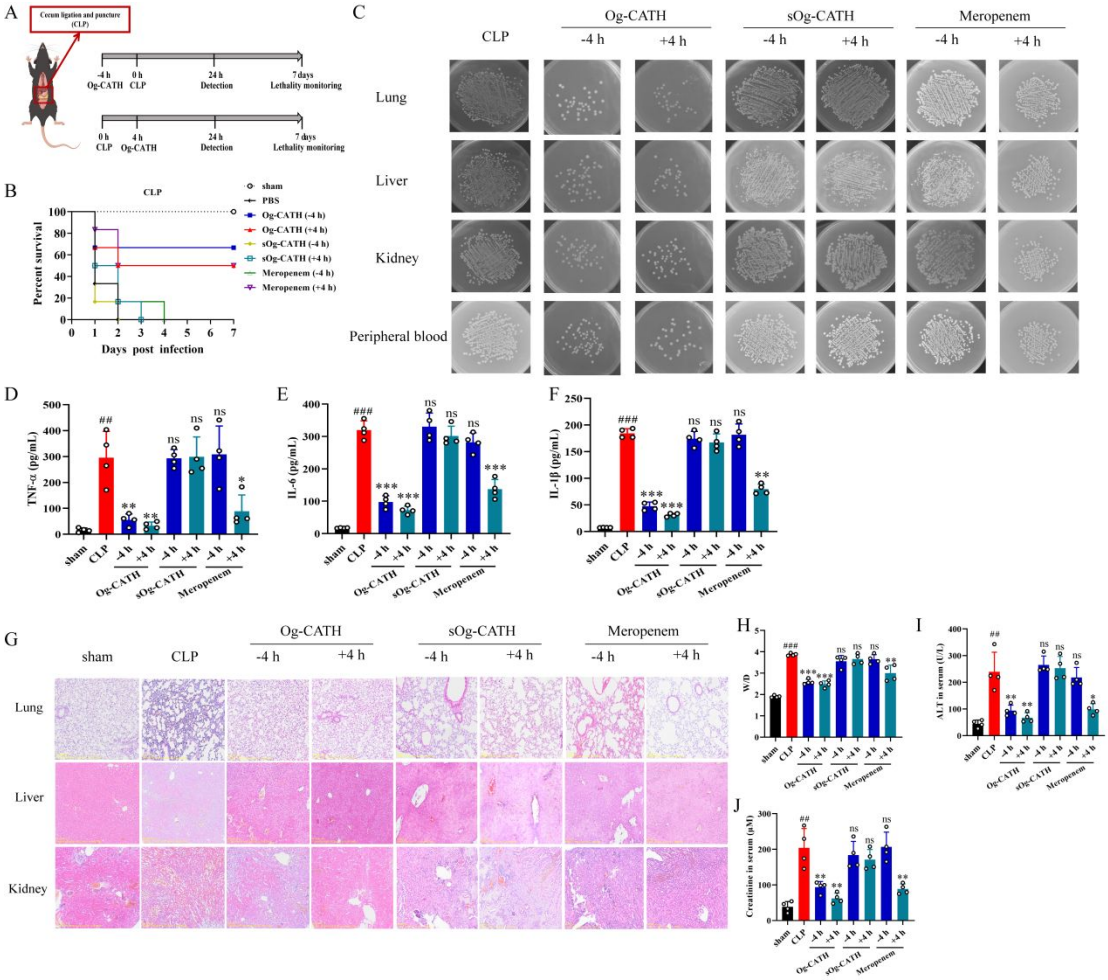

Figure 2 Og-CATH provides preventive and therapeutic effects against sepsis and sepsis-induced multiple organ dysfunction.

Male C57BL/6 mice (n = 6) received the intraperitoneal injection of 10 mg/kg Og-CATH, sOg-CATH (10 mg/kg) or Meropenem (10 mg/kg) 4 h prior to (–4 h) or 4 h (+ 4 h) after CLP operation. A: Scheme of the experimental workflow. B: The 7-days survival rates of CLP-induced septic mice after Og-CATH, sOg-CATH or Meropenem administration. Bacterial burden (C), and histopathological staining (G) of viscera (kidney, liver and lung) and peripheral blood, scale bar: 200 μm. D-F: cytokines levels in serum. H: Lung tissue wet/dry ratio. I, J: Serum ALT and creatinine levels. #represent statistical differences between the sham group and CLP group. All other groups were compared with the CLP group, and *represents statistical

differences between the groups. ## $P < 0.01$, ### $P < 0.001$; ** $P < 0.01$, *** $P < 0.001$, ns, no significant difference. n = 6 mice were used per group for survival studies. For endpoint analyses (bacterial burden, cytokines, histology), data from $n = 4$ mice per group are presented as the mean ± SD.

Og-CATH induces phagocytes influx in both frog and mice, and its protection in mice depends on monocytes/macrophages and neutrophils

After microbial infection, the successful clearance of pathogens depends on the migration of phagocytes to the site of infection (Bhuiyan *et al.*, 2016). We found that leukocyte influx was significantly enhanced in both the abdominal cavity of frogs (Figure 3A, B) and mice following Og-CATH (10 mg/kg) injection. In mice, Og-CATH primarily attracted neutrophils and inflammatory monocytes/macrophages, and peaked at 12 h and 24 h after injection (Figure 3C, D). But sOg-CATH and antibiotic meropenem did not show any chemotactic activity for neutrophils and macrophages (Figure 3E). To verify if Og-CATH's protection *in vivo* relies on these phagocytes, the anti-infective ability *in vivo* of Og-CATH was assessed in models of monocyte/macrophage or neutrophil elimination, induced by liposomes or cyclophosphamide, respectively. The result showed that after the injection of liposomes or cyclophosphamide, the chemotactic effect of Og-CATH on mononuclear/macrophages (Figure 3F) or neutrophils in the abdominal cavity of mice was significantly weakened (Figure 3G). Moreover, intraperitoneal administration of 10 mg/kg Og-CATH 4 h before or after CLP surgery failed to decrease the bacterial counts in peripheral blood of macrophage- (Figure 3H) or neutrophil-depleted septic

mice (Figure 3I).

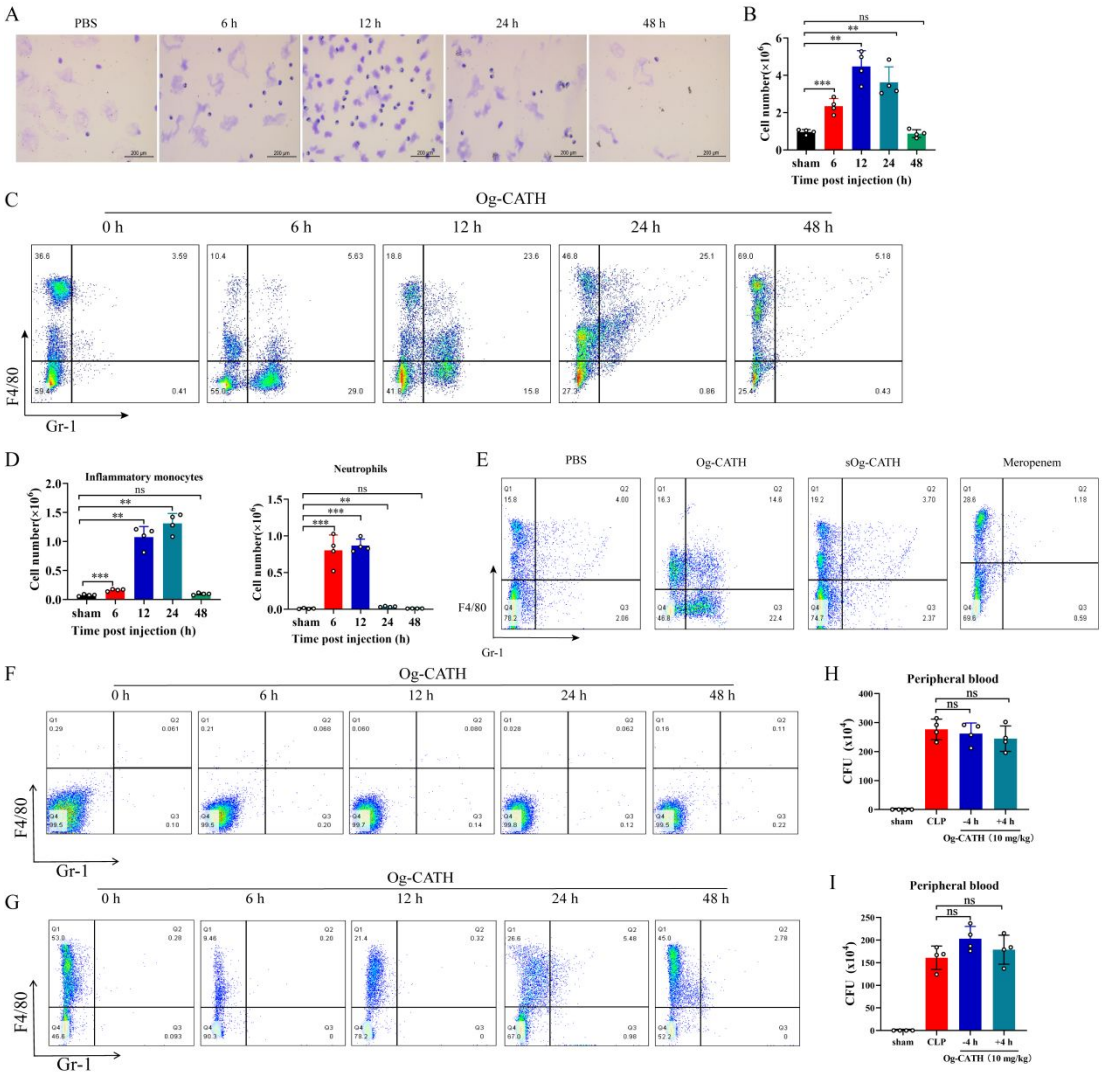

Figure 3 Og-CATH induces phagocytes influx in both frog and mice, and neutrophils and monocytes/macrophages are essential for the protective effect of Og-CATH in mice

A, B: *O. grahami* (21-30 g, n = 4) were given Og-CATH (10 mg/kg) via intraperitoneal injection. Peritoneal lavage cells were counted and examined at 6, 12, 24, and 48 h post-injection using Wright-Giemsa staining, scale bar: 200 μm. C, D: Analysis of cell types in the peritoneal lavage fluid of mice following Og-CATH administration, with representative flow cytometry plots (C) and quantitative analysis (D) of neutrophils and inflammatory monocytes shown. E: Analysis of cellular composition in the peritoneal lavage fluid of mice following

sOg-CATH and antibiotic meropenem administration, with representative flow cytometry plots. F, G: Macrophage (F) or neutrophils (G) deficient mice (n = 4) were intraperitoneally injected with Og-CATH (10 mg/kg). Peritoneal cells were collected and analyzed by flow cytometry. H, I: Bacterial counts in peripheral blood from monocyte/macrophage-depleted (H) and neutrophil- depleted septic mice (I). ** $P < 0.01$, *** $P < 0.001$, ns, no significant difference. Data represent the mean ± SD of four mice.

Og-CATH mediates the phagocyte migrations through P2X7 receptor on macrophages

Since Og-CATH demonstrated chemotactic effects on neutrophils and monocytes/macrophages in both frogs and mice, we assessed if Og-CATH functions as neutrophil and macrophage's direct chemoattractant. Supplementary Figure S5 showed that the migration of macrophages and neutrophils was not observed when treated with 100 μg/mL Og-CATH, suggesting that Og-ACTH itself does not possess the ability to directly attract neutrophils and macrophages. We next examined whether Og-CATH attracts neutrophils and macrophages when macrophages are present. As depicted in Figure 4A, B, Og-CATH stimulated the migration of phagocytes (macrophages and neutrophils) in a dose-dependent manner when macrophages were present.

It has been reported that macrophages can release chemokines that attract other immune cells to the infection site. To verify if Og-CATH-induced phagocyte migration depended on chemokine production by macrophages, we treated macrophages with Og-CATH (100 μg/mL), sOg-CATH (100 μg/mL) or meropenem (1 mg/mL) for 6 h, and examined the mRNA and protein levels of chemokines. The qPCR analysis revealed

that the gene levels of CXCL1, CXCL2, CXCL3 and CCL2 were markedly up-regulated by 40-, 19.0-, 18.0-, and 9.0-fold in macrophages with Og-CATH treatment relative to PBS-treated cells, and the other chemokines levels including CXCL5, CXCL7, CXCL10, CXCL11, and CXCL14 and CCL1, CCL3, CCL4, and CCL6 were slightly up-regulated by 1.0- to 5-fold (Figure 4C). Similarly, as depicted in Figure 4D, macrophages treated with Og-CATH showed a remarkable increase in the protein levels of CXCL1, CXCL2, CXCL3, and CCL2. Moreover, intraperitoneal administration of Og-CATH (10 mg/kg) also up-regulated the expression of CXCL1, CXCL2, CXCL3, and CCL2 ~~chemokines~~ in the mouse peritoneal lavage (Figure 4E). The same effect was observed in THP1 cells, Og-CATH markedly promoted the secrets of CXCL1, CXCL2, and CCL2 chemokines in macrophages (Supplementary Figure S6). However, the levels of these chemokines was no significant increased by sOg-CATH and antibiotic meropenem under the same conditions (Figure 4C). To understand the potential receptor that Og-CATH induced phagocytes migration, we evaluated the role of some chemotactic related receptor (P2X7 receptor, formyl peptide receptor-like 1, TLR4/MD2) in macrophages. As illustrated in Figure 4F, P2X7 receptor inhibitor (KN62) pre-treatment was markedly blocked Og-CATH-induced CXCL1, CXCL2, CXCL3 and CCL2 production in macrophages, while formyl peptide receptor-like 1 antagonist (WRW4) and anti-mouse TLR4/MD2 Ab (MTS510) treatment has no significantly impact on these chemokines' production.

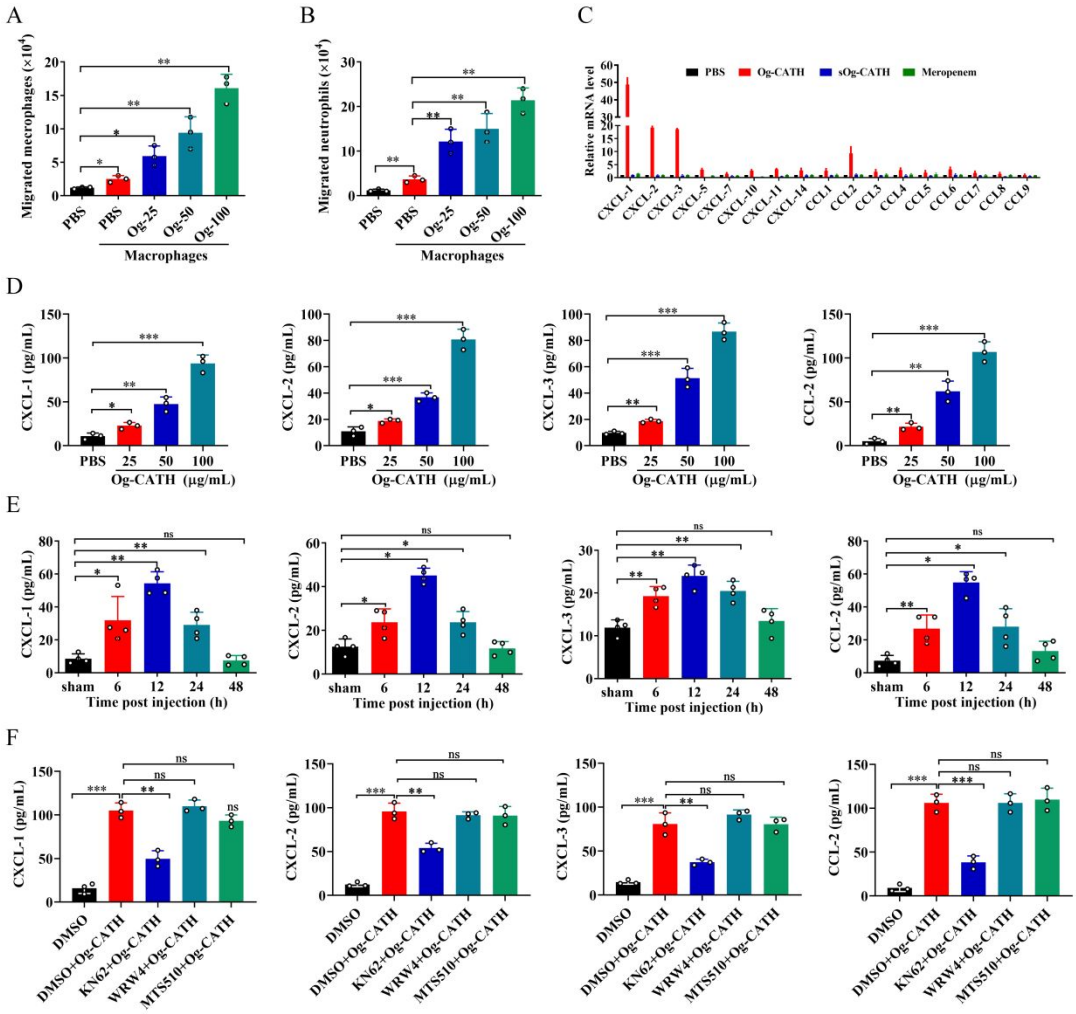

Figure 4 Og-CATH promotes phagocyte migrations via P2X7 receptor on macrophages

A, B: Indirect chemotaxis effect investigations on macrophage or neutrophil were performed in the presence of macrophages using co-culture system *in vitro*. The migrated cells were detected by assessing the reduced number of cells in the upper chamber. C: qPCR analysis of CXCL-and CCL-chemokines gene levels in macrophages. D, E: CXCL1, CXCL2, CXCL3, and CCL2 levels in cultured macrophage supernatants (D) and mouse peritoneal lavage (E). CXCL1, CXCL2, CXCL3, and CCL2 levels in supernatant (F) after macrophages were exposed to some related-receptor inhibitors. * $P < 0.05$, ** $P < 0.01$, *** $P < 0.001$, ns, no significant difference. Data represent the mean ± SD of triplicate experiments.

Og-CATH promotes phagocytosis and degranulation of neutrophils

Neutrophils can recognize, phagocytose and kill any invade microbes using effector mechanisms that phagocytosis and release of reactive oxygen species (ROS), nitrogen monoxide (NO), neutrophils extracellular traps (NETs) and endogenous antimicrobial molecules (Papayannopoulos, 2018; Andrés *et al.*, 2022). As shown in Figure 5, Og-CATH (100 μg/mL) markedly enhanced the phagocytic uptake of fluorescence-tagged *S. aureus* (Figure 5B) and *E. coli* (Figure 5B) in neutrophils in contrast to the PBS or sOg-CATH-treated group. We next also examined the non-oxidative (degranulation) and oxidative (ROS, NO, and NETs) killing of neutrophils. As illustrated in Figure 5C-E, Og-CATH exhibited no significant impact on the generation of ROS, NO, and NETs. However, Og-CATH dose-dependently enhanced release of intracellular bactericidal/permeability-increasing protein (BPI) and lactoferrin in neutrophils with compared to the sOg-CATH-treated group (Figure 5F).

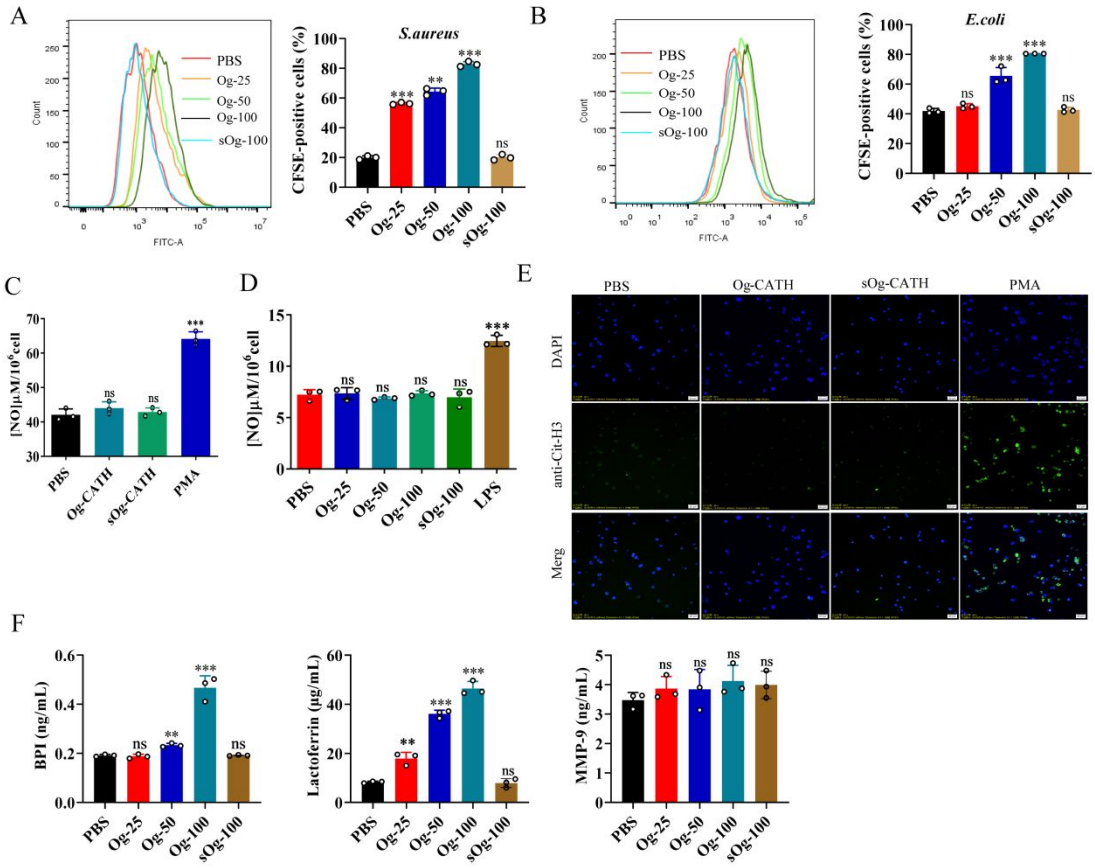

Figure 5 Og-CATH promotes neutrophils phagocytosis, and induces endogenous antimicrobial molecules release

A, B: Neutrophils were pre-incubated with 100 μg/mL Og-CATH, sOg-CATH (100 μg/mL) or PBS for 2 h, followed by incubation with CFSE-labeled *S. aureus* (A) and *E. coli* (B) for the specified times. Flow cytometry was used to analyze the CFSE fluorescence, which served as an indicator of the bacterial particles' phagocytic uptake. C: Neutrophils were treated with PMA (positive control), Og-CATH (100 μg/mL), sOg-CATH (100 μg/mL) or PBS were incubated at 37°C, followed by DCFH-DA (5 μM) staining. The ROS levels were multiple of the average fluorescence intensity (MFI) of PBS treatment. D: For NO detection, the cells were treated with Og-CATH (100 μg/mL), sOg-CATH (100 μg/mL) or PBS at 37℃ for 6 h, and NO levels in the supernatants were quantified using NO assay kits. E: Neutrophils were treated with PBS, Og-

CATH (100 μg/mL), sOg-CATH (100 μg/mL) or PMA for the indicated time, then stained with DAPI (blue) or anti-CitH3 (green) and examined for NET formation by confocal microscopy, scale bar= 20 μm. F: Lactoferrin, BPI and MMP-9 levels in neutrophils. ** $P < 0.01$, *** $P < 0.001$, ns, no significant difference. All groups were compared with PBS-treated group. Data represent the mean ± SD of triplicate experiments.

Og-CATH exhibits anti-thrombotic ability with no bleeding complications in mice

In addition to bacterial overgrowth due to an impaired phagocytic and bactericidal ability of immune cells, sepsis is always accompanied by alterations in both systemic and intra-alveolar coagulation, and in fibrinolysis (Bastarache *et al.*, 2006). Given that its role in the prevention and treatment of sepsis, the impact of Og-CATH on the pulmonary fibrin deposition in septic mice was also assessed. As shown in Figure 6A, the lungs showed massive fibrin deposits at 24 h post-CLP, and pre- or post-operative Og-CATH (10 mg/kg) injection reduced the deposition. We further investigated the anti-coagulation effect of Og-CATH on $FeCl_3$-induced carotid and carrageenan-induced tail thrombosis. As shown in Figure 6B, C, the blood flow in the untreated carotid artery was fully occluded within 10 min of 10% $FeCl_3$ solution treatment, however, intraperitoneal injection of heparin and Og-CATH (10 mg/kg) markedly delayed occlusion time to 23 ± 2 and 28.5 ± 1.5 min, respectively. Consistently, the administration of heparin (1000 U/kg) and Og-CATH (10 mg/kg) also ameliorated the length of the mouse tail thrombus induced by carrageenan (Figure 6D), and in contrast to sham group, sOg-CATH and antibiotic meropenem had no significant effect on the tail and carotid artery thrombosis in mice (Figure 6B-D). Meanwhile, a mouse tail

transection model and skin bleeding model were performed to assessed if Og-CATH induces bleeding complications in mice. Figure 6E showed the administration of Og-CATH (10 or 30 mg/kg) did not induce tail bleeding. A similar result was observed in a mouse skin bleeding model that 30 mg/kg of Og-CATH showed no effect on visible skin bleeding (Figure 6F, G). But in these cases, injection of 1000 U/kg heparin increased visible bleeding in skin and markedly prolonged the tail bleeding time (Figure 6E-G).

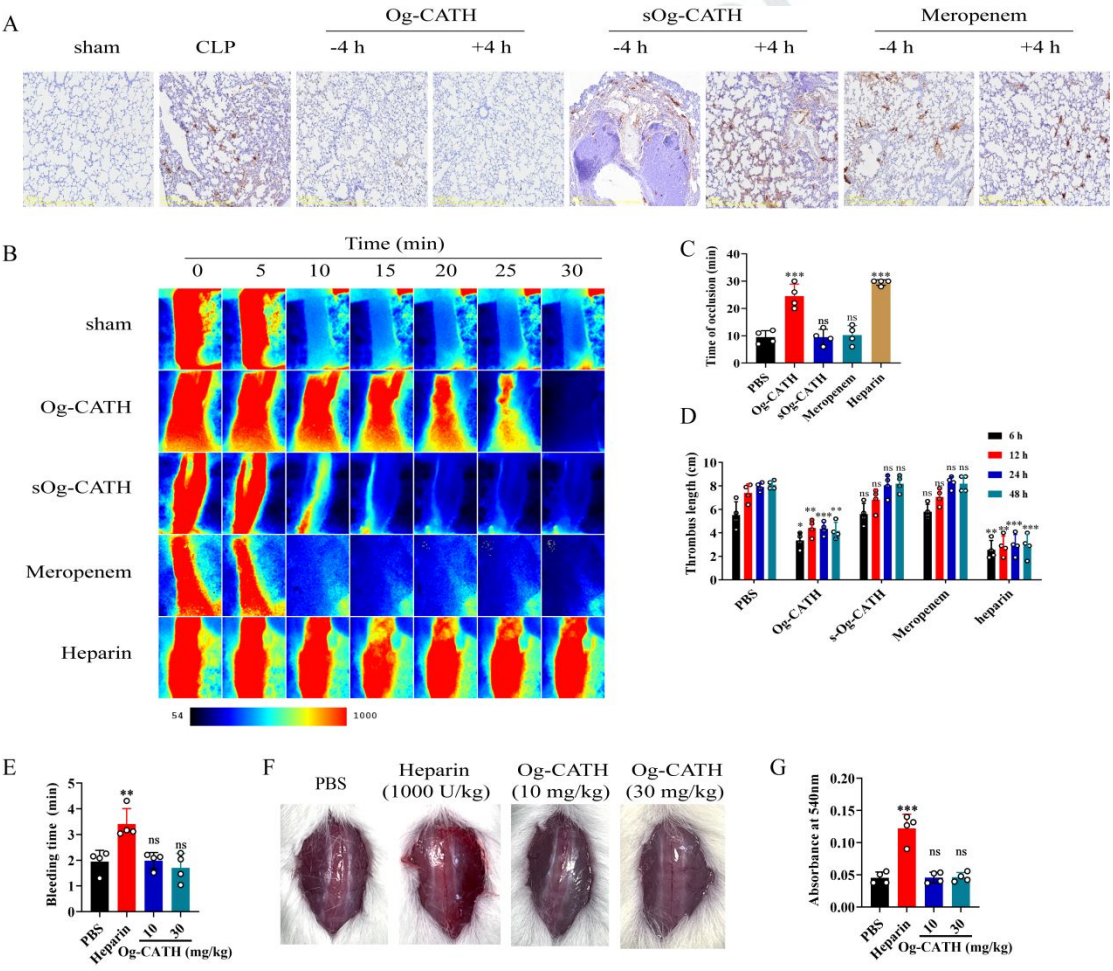

Figure 6 Og-CATH inhibits thrombosis *in vivo* and did not induce spontaneous bleeding complications in mice

A: Analysis of immunohistochemical in the lung tissue after intraperitoneal injection of Og-CATH (10 mg/kg), sOg-CATH (10 mg/kg) or Meropenem (10 mg/kg) 4 h before or after CLP operation, scale bar: 200 μm, n = 4. B, C: Representative traces of carotid artery blood flow (B) and quantitation (C) are shown. Positive control: Heparin (1000 U/kg). D: Statistical analysis of the length of the mouse tail thrombus induced by carrageenan. Positive control: Heparin (1000 U/kg), n = 6. E: At 20 min after Og-CATH (10 or 30 mg/kg) or Heparin (1000 U/kg) administration, the tails of mice were cut approximately 2 mm from the tip and immediately placed in saline. Time from initiation to termination of bleeding was monitored. F, G: Og-CATH (10 or 30 mg/kg) or Heparin (1000 U/kg, positive control) were applied intraperitoneally 1 h before mouse skin bleeding model was established, n = 6. Representative traces of skin wounds (F) and quantitation (G) are shown. * $P < 0.05$, ** $P < 0.01$, *** $P < 0.001$, ns, no significant difference. All groups were compared with PBS-treated group. Data represent the mean ± SD of four mice.

Og-CATH regulates the hemostatic balance by decreasing TF expression and increasing APC production in endothelial cell

Platelets and coagulation factors play a key role in the development of coagulation abnormalities in sepsis, and their activation may stimulate fibrin formation by alternative mechanism (Levi and van der Poll, 2017). To investigate the potential anti-thrombin mechanism of Og-CATH, the effects of Og-CATH on re-calcification time, PT (prothrombin time), aPTT (activated partial thromboplastin time) and platelet aggregation were detected *in vitro*. As indicated in Supplementary Figure S7, Og-

CATH (100 μg/mL) did not delay plasma re-calcification time, PT and aPTT (Supplementary Figure S7A, B) and did also not inhibit ADP-, college- or PMA-induced platelet aggregation (Supplementary Figure S7C).

Endothelial cells provide an anticoagulant environment by producing anticoagulant molecules to limit thrombin generation. However, the endothelium switches from an anti-thrombotic to a pro-thrombotic state during sepsis, which is critical factors in the development of thrombosis and organ failure (Pilard *et al.*, 2022). Therefore, we examined the regulatory effect of Og-CATH on endothelial anti-coagulation function in LPS-induced HUVEC. LPS at a concentration of 10 μg/mL was used to induce endothelial cell injury, resulting in a 30.85% reduction in cell viability (Supplementary Figure S8). Western bolt results showed that the expression of pro-coagulation tissue factor (TF) was increased after 24 h LPS stimulation, and the expression of anti-coagulation activated protein C (APC) in HUVEC was decreased significantly, compared with the control group (Figure 7A, B). However, the treatment of Og-CATH, but not sOg-CATH and meropenem (Supplementary Figure S9), significantly inhibited TF production and enhanced the expression of APC in LPS-induced HUVEC. APC exerts anticoagulant/antithrombotic effects by complex molecular pathways which have been demonstrated in various reviews. Endothelial protein C receptor (EPCR) and TM are the two important players of the endothelium anticoagulation system that controls APC expression (de Wouwer *et al.*, 2004; Nan *et al.*, 2005). As demonstrated in Figure 7A, B, the administration of Og-CATH markedly up-regulated the protein expression of TM and EPCR compared with the PBS treatment

group. Similar result were observed in the lung tissue of septic mice that intraperitoneal injection of Og-CATH (10 mg/kg), whether before or after-CLP operations, significantly decreased the TF generation and increased APC, TM and EPCR expression levels (Figure 7C, D). However, q-PCR data illustrated that Og-CATH had no remarkably effects on the expression of uPA and PAI-1 (Figure 7E), indicating it did not directly target fibrinolytic systems.

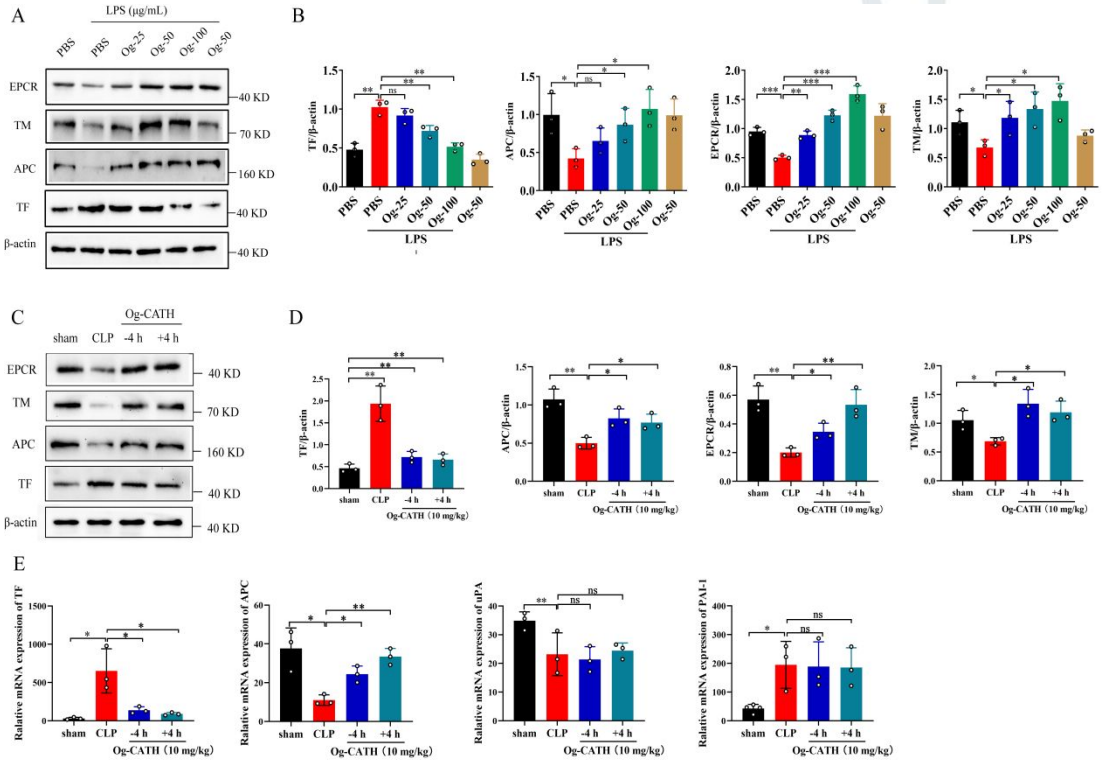

Figure 7 Og-CATH promotes the hemostatic balanc in endothelial cell and septic mice

A-E: HUVEC were treated with Og-CATH (25, 50, and 100 μg/mL) or PBS with/without LPS (10 μg/mL), then incubated at 37°C for 24 h. Representative WB images (A) and statistical analysis (B) of EPCR, TM, APC and TF proteins. C, D: Analysis of western blot in the lung tissue after intraperitoneal injection of Og-CATH 4 h before or after CLP operation. Representative WB images (C) and statistical analysis (D) of EPCR, TM, APC and TF proteins. E: qPCR analysis of TF, APC, uPA and PAI-1 gene levels in the lung tissue after intraperitoneal

injection of Og-CATH 4 h before or after CLP operation. * $P < 0.05$, ** $P < 0.01$, *** $P < 0.001$, ns, no significant difference. Data represent the mean ± SD of triplicate experiments.

Og-CATH enhances endothelial barrier *in vitro* and *in vivo*

In addition to the weakened anticoagulant activity of endothelial cells, endothelial dysfunction during sepsis is also typically manifested by endothelial barrier damage including endothelium inflammation, endothelial cell apoptosis, and disruption of endothelial junction proteins (Giannotta *et al.*, 2013; Kuo *et al.*, 2022). We next tested the effect of Og-CATH on endothelial barrier functions in LPS-induced HUVEC. As indicated in Figure 8A, Og-CATH markedly suppressed the production of inflammatory cytokines (TNF-α, IL-6, and IL-β) induced by LPS in a dose-dependent manner. Meanwhile, Flow cytometry showed that LPS markedly increased the percentage of endothelial cell apoptosis (19.4%), but Og-CATH dose-dependently reduced this apoptosis stimulated by LPS (Figure 8B). Additionally, Fig 8C showed that LPS exposure reduced ZO-1, occludin, and E-cadherin levels in HUVEC compared to control. However, these proteins ratio were significantly increased by Og-CATH. We also found similar results in lung from septic mice that Og-CATH (10 mg/kg) given 4 h before or after CLP increased ZO-1, occludin, and E-cadherin levels in lung tissue of septic mice (Figure 8D).

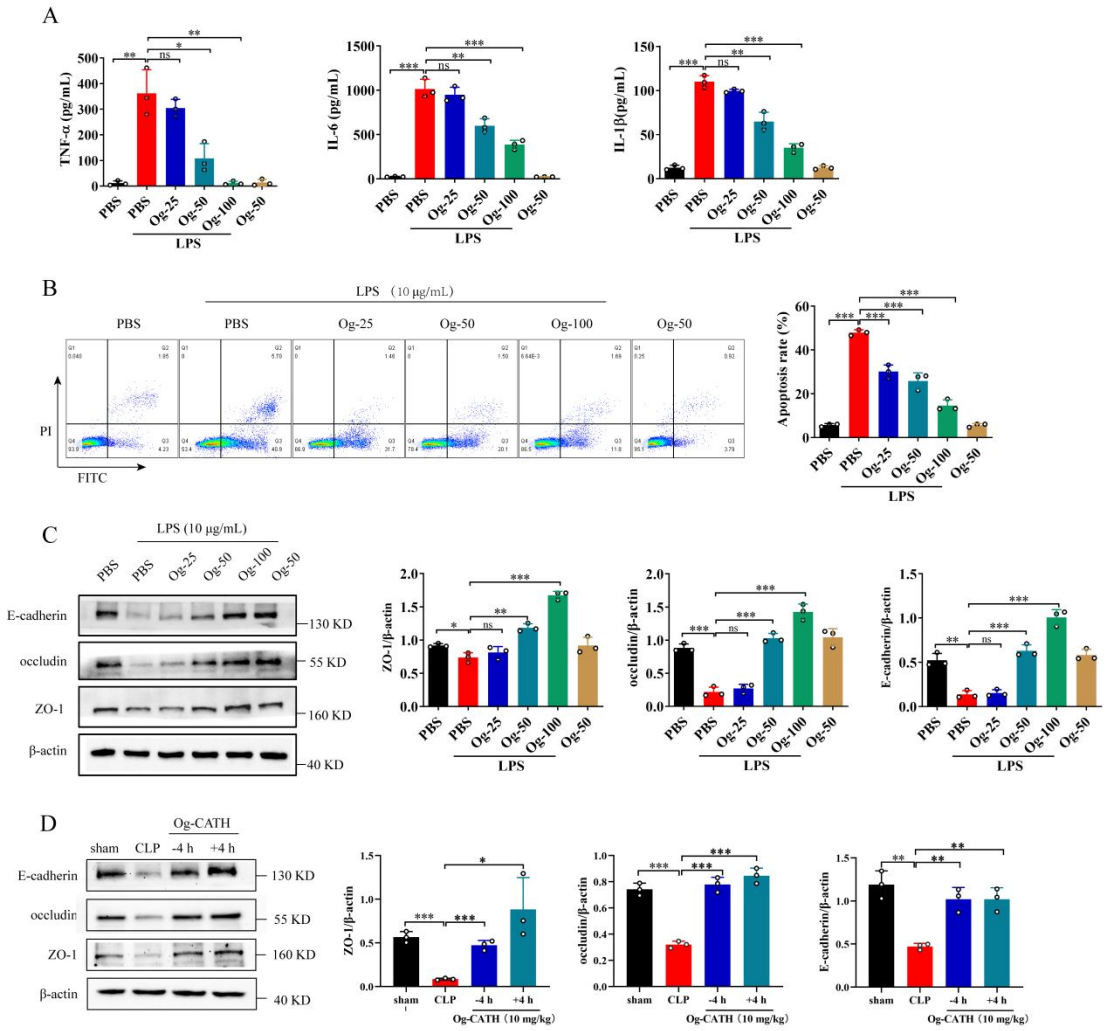

Figure 8 Og-CATH improves endothelial injury *in vitro* and *in vivo*

A-E: HUVEC were treated with Og-CATH (25, 50, and 100 μg/mL) or PBS, with or without LPS (10 μg/mL) , then incubated at 37°C for 24 h. A: TNF-α, IL-1β, and IL-6 levels from the supernatants. B: Cell apoptosis were assessed by flow cytometry analysis, representative images and statistical analysis were shown. C: Representative WB images and statistical analysis of ZO-1, occludin, and E-cadherin proteins. D: Mice received an intraperitoneal injection of Og-CATH (10 mg/kg) or PBS 4 h before or after the operation. ZO-1, occludin, and E-cadherin proteins levels assay in lung tissues from septic mice at indicated time points. * $P < 0.05$, ** $P < 0.01$, *** $P < 0.001$, ns, no significant difference. Data represent the mean ± SD of triplicate experiments.

Og-CATH specifically targets the MD2 protein and inhibits TLR4 signaling in endothelial cell

LPS sends proinflammatory signals primarily through TLR4. MD2, a co-receptor of TLR4, is responsible for ligand recognition. To explore the molecular target of Og-CATH action, we first used SPR to evaluate direct interaction between Og-CATH and LPS, TLR4 or MD2. As shown in Figure 9A, Og-CATH showed very strong binding response to MD 2 protein, with the KD values of 1.23 μM. However, no direct interaction observed between Og-CATH and LPS or TLR4. Similarly, ITC (isothermal calorimetry) assay results showed that the binding affinity of Og-CATH for MD2 is 0.142 μM (Figure 9B). Although the binding affifinities determined by SPR were slightly different from ITC assays, this is not surprising considering that the underlying principles of these two methods are different: SPR reflects the kinetics of binding and dissociation, whereas ITC directly measures the thermodynamics of the binding process. The molecular docking results further confirmed that Og-CATH had a good binding capacity with the MD2 protein (Figure 9C). Next, cellular thermal shift assay (CETSA) experiments were performed to support the direct interaction of Og-CATH with MD2. The results showed Og-CATH binding increased MD2 stability in HUVEC (Figure 9D). Notably, Og-CATH increased the Tm value of MD2 in HUVEC by 11.4℃.

Given the fact that Og-CATH significantly inhibited LPS-induced signaling and the downstream pro-inflammatory factors in the HUVEC, we investigated its effect on TLR4 signaling. The co-immunoprecipitation experiments were performed and the results showed that Og-CATH inhibited the LPS-induced MyD88 recruitment to

TLR4 and suppressed the formation of the TLR4/MD2/MyD88 complex (Figure 9E, F). Moreover, LPS stimulation signifificantly upregulated the phosphorylation of IKKα/β, p65, and IKB-α, but Og-CATH inhibited the LPS-induced phosphorylation of these TLR4 signaling factors (Figure 9G, H). Given that immune cells may be more sensitive in response to LPS both *in vitro* and *in vivo*, we also investigated the effect of Og-CATH on the expression of inflammatory cytokines in LPS-induced mouse peritoneal macrophages and human monocytic THP-1 cells, data showed that Og-CATH significantly inhibited the production of TNF-α in these cells (Supplementary Figure S10), indicating that it may indirectly alleviate endothelial damage by suppressing the immune cell-mediated cytokine storm. However, LPS also binds with endothelial cells and upregulates adhesion molecules and tissue factor in a MyD88-dependent fashion, which are critical for the coagulation and vasodilatation. Our results showed that Og-CATH does not act directly on LPS or its receptor TLR4, indicating that it can directly target endothelial cells to modulate their functional state, rather than merely providing indirect protection by reducing cytokine production from immune cells.

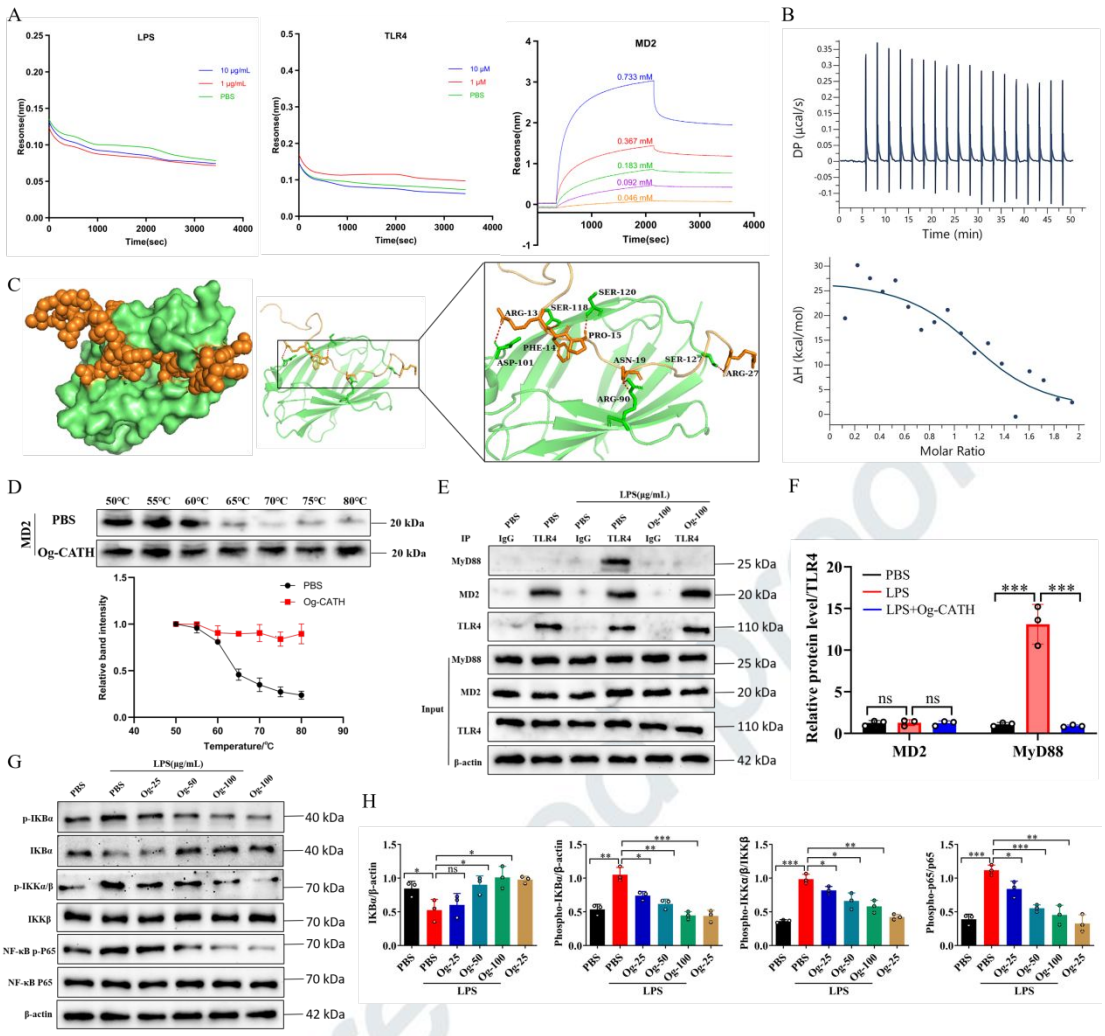

Figure 9 Og-CATH targets MD2 protein and inhibits TLR4 signaling in endothelial cell

A: The interaction of Og-CATH with LPS , TLR4 or MD2 was investigated using a FortéBio ´ Octet system. Og-CATH (100 μg/mL) was immobilized on sensor tips, and varying concentrations of LPS (1 and 10 μg/mL), TLR4 (1 and 10 μM), or MD2 (0.046-0.733 mM) were tested. B: ITC analysis showing the binding of Og-CATH to MD2. C: Molecular docking analysis of Og-CATH with the TLR4/MD2 complex (PDB:3FXI), and the potential interaction binding site. D: Cellular thermal shift assay of MD2 with Og-CATH. Og-CATH binding increases MD2 thermal stability (ΔTm = 11.4 ℃). E, F: HUVECs were treated with LPS (10 μg/mL) and Og-CATH (100 μg/mL) for 1 h. Co-immunoprecipitation was performed using an anti-TLR4 antibody, and MD2, TLR4, and MyD88 were detected by western blotting. G, H:

The effect of Og-CATH on the LPS-induced phosphorylation of IKBα, IKKβ, and p65. * $P <$ 0.05, ** $P < 0.01$, *** $P < 0.001$, ns, no significant difference. Data represent the mean ± SD of triplicate experiments.

DISCUSSION

Despite substantial advancements in our knowledge of the pathophysiology of sepsis, numerous clinical trials have been unsuccessful in identifying novel therapies or drugs (Gauer *et al.*, 2020). Novel drugs for the treatment of bacterial sepsis are urgently needed. Herein, we identified a new cathelicidin host defence peptide (Og-CATH) from the *O. grahami* skin. Og-CATH is a short cationic peptide composed of 28 amino acid residues, and showed no direct antimicrobial activity *in vitro*. Notably, intraperitoneal administration of Og-CATH either prior to or after infection improved survival in septic mice caused by a lethal dose of bacterial inoculation or cecal ligation and puncture (CLP). Additionally, in the polymicrobial mouse model of intra-abdominal sepsis, Og-CATH reduced the systemic inflammatory response and mitigated multipleorgan (lung, liver, and kidney) injuries. But the scrambled version of Og-CATH (sOg-CATH) did not show any significant improvement in the survival of septic mice, indicating that Og-CATH seems to be a specific anti-infective peptide.

Previous studies have found variable results that extended immunosuppression in sepsis patients can leave them susceptible to secondary infection and mortality. The change in preference from immunosuppressive treatments to immunostimulatory drugs has also shown promising effects in animal models and preclinical studies. Neutrophils and monocytes/macrophages are two major phagocytes that play essential roles

in the innate immune system, diminished macrophages and neutrophil activation or decreased cells numbers are associated with a high mortality rate in sepsis (Zhang *et al.*, 2023). In our current study, Og-CATH effectively promoted leukocyte influx in *O. grahami*, and induced neutrophil and monocytes/macrophages migration in mice. Furthermore, *in vivo* experiments implicated macrophages/monocytes and neutrophils are key effector cells of Og-CATH, because its protective effects were significantly decreased in macrophage or neutrophil-depleted septic mice. These results indicated that Og-CATH is likely to exert its anti-infective effect as a regulator of immune effector functions. However, unlike some bactericidal cationic immunomodulatory peptide, e.g. LL-37, which directly recruit phagocytes to infection sites to eliminate bacterial pathogens (Tjabringa *et al.*, 2006), Og-CATH indirectly attracted neutrophils and monocytes/macrophages by stimulating P2X7 receptor-mediate CXCL-1, CXCL-2, CXCL-3 and CCL-2 chemokines release in macrophages. Neutrophils are professional phagocytes, and it kill any available microbes at the sites of infection (Herro and Grimes, 2024). NADPH oxygen-dependent killing activity, including ROS release and NETs generations, were considered the predominant mechanisms by which cationic host defence peptide combat invasive pathogens (Shi *et al.*, 2022; Yang *et al.*, 2022; He *et al.*, 2023; He *et al.*, 2024). However, our data indicated Og-CATH showed no significant effect on oxidative killing activities of neutrophils. Intriguingly, it significantly enhanced the phagocytosis of neutrophils, and induced its degranulation to release endogenous antimicrobial molecules (BPI and Lactoferrin), suggesting that Og-CATH indirectly eliminated bacteria by enhancing neutrophils-mediated oxygen-

independent killing.

Although the effective clearance of invading bacterial pathogens are the key to improving the prognosis of sepsis, it is recognized that antibiotic treatment alone is unable to treat sepsis effectively, as sepsis is a complex syndrome involving multi-organ dysfunction. Central to the pathophysiology of sepsis, endothelial cells play a critical role in regulating hemostatic balance and maintaining barrier integrity across various organs and tissues (Joffre *et al.*, 2020; Zhang *et al.*, 2023). Nevertheless, most of the previous work on cationic host defence peptide have focused on the regulation of the host innate immune and inflammatory response (Li *et al.*, 2013; Cai *et al.*, 2018; Nagaoka *et al.*, 2020; Wu *et al.*, 2021), less information is available about their regulatory functions on the vascular endothelium during sepsis. In this study, intraperitoneal administration of Og-CATH either prior or post infection effectively decreased the widespread deposition of pulmonary fibrin, suggesting it could mitigate haematological abnormalities in septic mice. This antithrombotic effect was further confirmed in $FeCl_3$-induced arterial thrombosis and carrageenan-induced tail vein thrombosis models. Moreover, skin and tail bleeding experiments proved Og-CATH does not appear to increase bleeding risk, and this is a great advantage in anticoagulant therapy *in vivo*. Several previous studies have reported that host defence peptides can depress blood clotting via inhibition of serine proteases or platelet aggregation (Chai *et al.*, 2021; Wu *et al.*, 2021; He *et al.*, 2024), but our results showed Og-CATH does not delay re-calcification time, PT, or aPTT of normal plasma, nor did

it inhibit platelet aggregation *in vitro*. It is interesting that Og-CATH effectively inhibited procoagulant TF production in LPS-stimulated HUVEC, and increased the expression of anticoagulant APC by up-regulating TM and EPCR levels, which play an important role in guaranting regular production of circulating APC. Similar results were observed in the lung tissue of septic mice. These findings indicated that, although Og-CATH has no direct impact on platelet aggregation and serine protease activity in coagulation cascade, it effectively regulates the hemostatic balance during sepsis by a decreased TF expression and an increased APC production in endothelial cells. In addition, Og-CATH also attenuated endothelial dysfunction by inhibiting LPS-stimulated endothelial cell apoptosis and the release of pro-inflammatory cytokines (TNF-α, IL-6, and IL-1β), as well as up-regulating the expression of barrier associated proteins (ZO-1, occludin, and E-cadherin).

We further analyzed the key target and the signaling pathway through which Og-CATH act in endothelial cell. Molecular docking, SPR, ITC, and CETSA binding assays showed that Og-CATH is specifically recognized by the TLR4 accessory protein MD2 and has a strong binding affinity. In contrast, SPR results illustrated that direct recognition of LPS and TLR4 by Og-CATH appears unlikely. Upon LPS stimulation, the TLR4 dimerassociates with MD2 and forms a complex with CD14. Subsequently, the adaptor proteins MyD88 is recruited to the TLR and binds to the cytoplasmatic domain of TLR-4, thereby mediating downstream TLR signaling. In this study, co-immunoprecipitation experiment confirmed Og-CATH inhibited the LPS-induced MyD88 recruitment to TLR4 and suppressed the formation of the TLR4/MD2/MyD88

complex. Moreover, Og-CATH also reduced LPS-induced phosphorylation of TLR4 signaling factors including IKK, IKB-α, and p65 in HUVEC. To date, only human cathelicidin peptides LL-37 acts on endothelial cells to promote cell proliferation and maintains endothelial barrier permeability, thereby attenuating lethal sepsis/endotoxin shock or liver injury, but these studies did not define the intracellular targets or mechanisms of action of LL -37 in endothelial cells (Zhai *et al.*, 2020; Suzuki *et al.*, 2022). In the current study, we confirmed that Og-CATH target MD2 and inhibit the downstream TLR4 signal, thereby attenuateing endothelial injury in sepsis.The above results suggested that Og-CATH not only enhanced innate immune cells-mediated antimicrobial immunity but also alleviated endothelial injury during sepsis by targeting the MD2 protein. Furthermore, although meropenem significantly reduced the bacterial load in septic mice, our data confirmed that it had no significant effect on the functions of phagocytes and endothelial cells, as well as tail and carotid artery thrombosis in mice. However, under the same conditions, the administration of Og-CATH alone significantly prolonged the blood flow occlusion time and up-regulated the expression levels of APC in endothelial cells, indicating that the binding of Og-CATH to MD2 protein promoted the endothelium switches from a pro-thrombotic state to an anti-thrombotic. These results prove that the antithrombotic properties of Og-CATH are not merely secondary to the decrease of bacterial growth. Bacterial antibiotic resistance urgently requires the development of effective treatment strategies. In recent years, non-antibiotic compounds (such as immune regulatory peptides) have played an important role in the treatment of drug-resistant bacteria, and the combination of non-antibiotic

compounds with antibiotics is considered a promising strategy against MDR bacteria. The results of the primary analysis of the study implying Og-CATH may be a potentially promising candidate molecule that could be used in combination with antibiotics to combat microbial infections, which will be the focus of our future research.

In conclusion, we identified a novel cathelicidin AMP (Og-CATH) from the skin of *O. grahami*. Og-CATH showed no direct antimicrobial activity but exerted prophylactic and therapeutic efficacy against bacterial sepsis in mice. In addition to boosting innate antimicrobial immunity, Og-CATH also modulate endothelial barrier integrity and anticoagulant function by targeting MD2 and inhibiting TLR4 signal, mitigating the haematological abnormalities and organ dysfunction during sepsis. Moreover, Og-CATH showed good serum and salt stability and low cytotoxicity. The combination of these properties makes Og-CATH an excellent candidate for development as an anti-sepsis agent.

SUPPLEMENTAL INFORMATION

Supplementary material to this article can be found in the accompanying annex.

ACKNOWLEDGMENTS

This work was supported by National Natural Science Foundation of China (U24A20812, 82372259), Applied Basic Research Foundation of Yunnan Province (202501AS070024, 202301AY070001-015, 202401AY070001-219), Yunnan

Revitalization Talent Support Program (YUWR-QNBJ-2019-189) , First-Class Discipline Team of Kunming Medical University (2024XKTDYS01) and Yunnan Provincial Department of Education Science Research Fund Project (2024J0331, 2025J0156).

DECLARATION OF INTERESTS

The authors declare no competing interests.

AUTHORS' CONTRIBUTIONS

L.W, J.W., and H.L.Y. designed the study. Y.M.H., T.L., and L.X.M. performed the majority of experiments. X.Y.Z., Y.S., J.Y.Y., and H.Y.L. organized data and made figures. Y.M.H., T.L., and L.X.M. wrote the manuscript, L.W, J.W., and H.L.Y. revised the manuscript. All authors contributed to the manuscript revisions.

REFERENCE

Aird, W.C., 2001. Vascular bed-specific hemostasis: Role of endothelium in sepsis pathogenesis. Critical care medicine, 29(7 Suppl): S28-34; discussion S34-25. DOI 10.1097/00003246-200107001-00013.

Alford, M.A., B. Baquir, F.L. Santana, E.F. Haney and R.E.W. Hancock, 2020. Cathelicidin host defense peptides and inflammatory signaling: Striking a balance. Front Microbiol, 11: 1902. Available from https://www.ncbi.nlm.nih.gov/pubmed/32982998. DOI 10.3389/fmicb.2020.01902.

Andrés, C.M.C., J.M. Pérez de la Lastra, C.A. Juan, F.J. Plou and E.J.V. Pérez-Lebeña, 2022. The role of reactive species on innate immunity. 10(10): 1735.

Bastarache, J.A., L.B. Ware and G.R. Bernard, 2006. The role of the coagulation cascade in the continuum of sepsis and acute lung injury and acute respiratory distress syndrome. In: Seminars in respiratory and critical care medicine. Copyright© 2006 by Thieme Medical Publishers, Inc., 333 Seventh Avenue, New …: pp: 365-376.

Bhuiyan, M.S., F. Ellett, G.L. Murray, X. Kostoulias, G.M. Cerqueira, K.E. Schulze, M.H. Mahamad Maifiah, J. Li, D.J. Creek, G.J. Lieschke and A.Y. Peleg, 2016. Acinetobacter baumannii phenylacetic acid metabolism influences infection outcome through a direct effect on neutrophil chemotaxis. Proceedings of the National Academy of Sciences of the

United States of America, 113(34): 9599-9604. DOI 10.1073/pnas.1523116113.

Cai, S., X. Qiao, L. Feng, N. Shi, H. Wang, H. Yang, Z. Guo, M. Wang, Y. Chen, Y. Wang and H. Yu, 2018. Python cathelicidin cathpb1 protects against multidrug-resistant staphylococcal infections by antimicrobial-immunomodulatory duality. Journal of medicinal chemistry, 61(5): 2075-2086. DOI 10.1021/acs.jmedchem.8b00036.

Chai, J., X. Chen, T. Ye, B. Zeng, Q. Zeng, J. Wu, B. Kascakova, L.A. Martins, T. Prudnikova, I.K. Smatanova, M. Kotsyfakis and X. Xu, 2021. Characterization and functional analysis of cathelicidin-mh, a novel frog-derived peptide with anti-septicemic properties. eLife, 10. DOI 10.7554/eLife.64411.

de Wouwer, M.V., D. Collen, E.M.J.A. Conway, thrombosis, and v. biology, 2004. Thrombomodulin-protein c-epcr system: Integrated to regulate coagulation and inflammation. 24(8): 1374-1383.

Dejager, L., I. Pinheiro, E. Dejonckheere and C. Libert, 2011. Cecal ligation and puncture: The gold standard model for polymicrobial sepsis? Trends in microbiology, 19(4): 198-208. DOI 10.1016/j.tim.2011.01.001.

Gauer, R., D. Forbes and N. Boyer, 2020. Sepsis: Diagnosis and management. American family physician, 101(7): 409-418.

Giannotta, M., M. Trani and E.J.D.c. Dejana, 2013. Ve-cadherin and endothelial adherens junctions: Active guardians of vascular integrity. 26(5): 441-454.

He, Y., S. Ruan, G. Liang, J. Hao, X. Zhou, Z. Li, L. Mu, J. Wu and H. Yang, 2024. A nonbactericidal anionic antimicrobial peptide provides prophylactic and therapeutic efficacies against bacterial infections in mice by immunomodulatory-antithrombotic duality. Journal of medicinal chemistry, 67(9): 7487-7503. DOI 10.1021/acs.jmedchem.4c00342.

He, Y., Y. Shen, X. Feng, S. Ruan, Y. Zhao, L. Mu, J. Wu and H. Yang, 2023. Tree frog-derived cathelicidin protects mice against bacterial infection through its antimicrobial and anti-inflammatory activities and regulatory effect on phagocytes. ACS infectious diseases, 9(11): 2252-2268. DOI 10.1021/acsinfecdis.3c00316.

Herb, M. and M. Schramm, 2021. Functions of ros in macrophages and antimicrobial immunity. Antioxidants (Basel), 10(2). Available from https://www.ncbi.nlm.nih.gov/pubmed/33669824. DOI 10.3390/antiox10020313.

Herro, R. and H.L. Grimes, 2024. The diverse roles of neutrophils from protection to pathogenesis. Nature immunology, 25(12): 2209-2219. DOI 10.1038/s41590-024-02006-5.

Iba, T., J. Helms, M.D. Neal and J.H. Levy, 2023. Mechanisms and management of the coagulopathy of trauma and sepsis: Trauma-induced coagulopathy, sepsis-induced coagulopathy, and disseminated intravascular coagulation. Journal of thrombosis and haemostasis : JTH, 21(12): 3360-3370. DOI 10.1016/j.jtha.2023.05.028.

Izadpanah, A. and R.L. Gallo, 2005. Antimicrobial peptides. Journal of the American Academy of Dermatology, 52(3 Pt 1): 381-390; quiz 391-382. DOI 10.1016/j.jaad.2004.08.026.

Joffre, J., J. Hellman, C. Ince and H. Ait-Oufella, 2020. Endothelial responses in sepsis. American journal of respiratory and critical care medicine, 202(3): 361-370. DOI 10.1164/rccm.201910-1911TR.

Kawasaki, T. and T.J.F.i.i. Kawai, 2014. Toll-like receptor signaling pathways. 5: 461.

Kuo, W.T., M.A. Odenwald, J.R. Turner and L.J.A.o.t.N.Y.A.o.S. Zuo, 2022. Tight junction

proteins occludin and zo-1 as regulators of epithelial proliferation and survival. 1514(1): 21-33.

Lei, X., C. Zhi, W. Huang, X. Sun, W. Gao, X. Yin, X. Zhang, C. Liang, H. Zhang and F. Sun, 2020. Recombinant ganoderma lucidum immunomodulatory protein improves the treatment for chemotherapy-induced neutropenia. Frontiers in pharmacology, 11: 956. DOI 10.3389/fphar.2020.00956.

Levi, M. and T.J.T.r. van der Poll, 2017. Coagulation and sepsis. 149: 38-44.

Li, B., Z.P. Qi, D.L. He, Z.H. Chen, J.Y. Liu, M.W. Wong, J.W. Zhang, E.P. Xu, Q. Shi, S.L. Cai, D. Sun, L.Q. Yao, P.H. Zhou and Y.S. Zhong, 2021. Nlrp7 deubiquitination by usp10 promotes tumor progression and tumor-associated macrophage polarization in colorectal cancer. Journal of experimental & clinical cancer research : CR, 40(1): 126. DOI 10.1186/s13046-021-01920-y.

Li, S.A., Y. Xiang, Y.J. Wang, J. Liu, W.H. Lee and Y. Zhang, 2013. Naturally occurring antimicrobial peptide oh-cath30 selectively regulates the innate immune response to protect against sepsis. Journal of medicinal chemistry, 56(22): 9136-9145. DOI 10.1021/jm401134n.

Liu, X., L. Zeng, Y. Zhou, X. Zhao, L. Zhu, J. Zhang, Y. Pan, C. Shao and J. Fu, 2023. P21 facilitates macrophage chemotaxis by promoting ccl7 in the lung epithelial cell lines treated with radiation and bleomycin. Journal of translational medicine, 21(1): 314. DOI 10.1186/s12967-023-04177-5.

Mookherjee, N. and R.E. Hancock, 2007. Cationic host defence peptides: Innate immune regulatory peptides as a novel approach for treating infections. Cell Mol Life Sci, 64(7-8): 922-933. Available from https://www.ncbi.nlm.nih.gov/pubmed/17310278. DOI 10.1007/s00018-007-6475-6.

Mookherjee, N., L.M. Rehaume and R.E. Hancock, 2007. Cathelicidins and functional analogues as antisepsis molecules. Expert opinion on therapeutic targets, 11(8): 993-1004. DOI 10.1517/14728222.11.8.993.

Nagaoka, I., H. Tamura and J. Reich, 2020. Therapeutic potential of cathelicidin peptide ll-37, an antimicrobial agent, in a murine sepsis model. International journal of molecular sciences, 21(17). DOI 10.3390/ijms21175973.

Nan, B., H. Yang, S. Yan, P.H. Lin, A.B. Lumsden, Q. Yao and C.J.S. Chen, 2005. C-reactive protein decreases expression of thrombomodulin and endothelial protein c receptor in human endothelial cells. 138(2): 212-222.

Nedeva, C., 2021. Inflammation and cell death of the innate and adaptive immune system during sepsis. Biomolecules, 11(7). DOI 10.3390/biom11071011.

Papayannopoulos, V.J.N.R.I., 2018. Neutrophil extracellular traps in immunity and disease. 18(2): 134-147.

Pilard, M., E.L. Ollivier, V. Gourdou-Latyszenok, F. Couturaud and C.A.J.F.i.C.M. Lemarié, 2022. Endothelial cell phenotype, a major determinant of venous thrombo-inflammation. 9: 864735.

Rittirsch, D., M.S. Huber-Lang, M.A. Flierl and P.A. Ward, 2009. Immunodesign of experimental sepsis by cecal ligation and puncture. Nature protocols, 4(1): 31-36. DOI 10.1038/nprot.2008.214.

Segal, A.W., 2005. How neutrophils kill microbes. Annual review of immunology, 23: 197-223.

DOI 10.1146/annurev.immunol.23.021704.115653.

Shi, J., J. Wu, Q. Chen, Y. Shen, K. Mi, H. Yang and L. Mu, 2022. A frog-derived cathelicidin peptide with dual antimicrobial and immunomodulatory activities effectively ameliorates staphylococcus aureus-induced peritonitis in mice. ACS infectious diseases, 8(12): 2464-2479. DOI 10.1021/acsinfecdis.2c00260.

Strich, J.R., E.L. Heil and H. Masur, 2020. Considerations for empiric antimicrobial therapy in sepsis and septic shock in an era of antimicrobial resistance. The Journal of infectious diseases, 222(Suppl 2): S119-s131. DOI 10.1093/infdis/jiaa221.

Suzuki, K., M. Ohkuma, A. Someya, T. Mita and I. Nagaoka, 2022. Human cathelicidin peptide ll-37 induces cell death in autophagy-dysfunctional endothelial cells. Journal of immunology (Baltimore, Md. : 1950), 208(9): 2163-2172. DOI 10.4049/jimmunol.2100050.

Team, E.E., 2013. Cdc publishes report on antibiotic resistance threats in the united states for the first time.

Teng, T.S., A.L. Ji, X.Y. Ji and Y.Z. Li, 2017. Neutrophils and immunity: From bactericidal action to being conquered. J Immunol Res, 2017: 9671604. Available from https://www.ncbi.nlm.nih.gov/pubmed/28299345. DOI 10.1155/2017/9671604.

Tjabringa, G.S., D.K. Ninaber, J.W. Drijfhout, K.F. Rabe and P.S. Hiemstra, 2006. Human cathelicidin ll-37 is a chemoattractant for eosinophils and neutrophils that acts via formyl-peptide receptors. International archives of allergy and immunology, 140(2): 103-112. DOI 10.1159/000092305.

van der Poll, T. and R.I. Parker, 2020. Platelet activation and endothelial cell dysfunction. Critical care clinics, 36(2): 233-253. DOI 10.1016/j.ccc.2019.11.002.

Wu, J., H. Zhang, X. Chen, J. Chai, Y. Hu, W. Xiong, W. Lu, M. Tian, X. Chen and X. Xu, 2021. Fm-cath, a novel cathelicidin from fejervarya multistriata, shows therapeutic potential for treatment of clp-induced sepsis. Frontiers in pharmacology, 12: 731056. DOI 10.3389/fphar.2021.731056.

Xue, L., X. Jin, T. Ji, R. Li, X. Zhuge, F. Xu, Z. Quan, H. Tong and W. Yu, 2023. Luteolin ameliorates dss-induced colitis in mice via suppressing macrophage activation and chemotaxis. International immunopharmacology, 124(Pt B): 110996. DOI 10.1016/j.intimp.2023.110996.

Yang, H., B. Lu, D. Zhou, L. Zhao, W. Song and L. Wang, 2017. Identification of the first cathelicidin gene from skin of chinese giant salamanders andrias davidianus with its potent antimicrobial activity. Developmental and comparative immunology, 77: 141-149. DOI 10.1016/j.dci.2017.08.002.

Yang, Y., J. Wu, Q. Li, J. Wang, L. Mu, L. Hui, M. Li, W. Xu, H. Yang and L. Wei, 2022. A non-bactericidal cathelicidin provides prophylactic efficacy against bacterial infection by driving phagocyte influx. eLife, 11. DOI 10.7554/eLife.72849.

Zhai, T., J. Zhang, Y. Zhang and Y. Wu, 2020. Cathelicidin deficiency exacerbates cardiac dysfunction in lipopolysaccharide-induced endotoxaemic mice. Clinical and experimental pharmacology & physiology, 47(4): 677-686. DOI 10.1111/1440-1681.13234.

Zhang, H., Y. Wang, M. Qu, W. Li, D. Wu, J.P. Cata and C. Miao, 2023. Neutrophil, neutrophil extracellular traps and endothelial cell dysfunction in sepsis. Clinical and translational medicine, 13(1): e1170. DOI 10.1002/ctm2.1170.